2016

Characterisation of NanoDot optically stimulated luminescent dosimeters for in vivo radiotherapy dosimetry

Christopher Boyd
University of Wollongong, cb977@uow.edu.au

UNIVERSITY OF WOLLONGONG

Characterisation of NanoDot Optically Stimulated Luminescent Dosimeters for *In vivo* Radiotherapy Dosimetry

*A thesis submitted in partial fulfilment of the

requirements for the award of the degree

Masters of Science - Research

from

University of Wollongong

By

Christopher Boyd, BMedRadPhys

Faculty of Engineering and Information Sciences

2016

I CERTIFICATION

I, Christopher M. Boyd, declare that this thesis, submitted in partial fulfilment of the requirements for the award of Masters of Science by Research, in the faculty of Engineering, University of Wollongong, is wholly my own work unless otherwise referenced or acknowledged. The document has not been submitted for qualifications at any other academic institution.

Christopher M. Boyd

29th March 2016

To Laura,

Your smile lights up the world.

Reminding me nothing worth

Being proud of was ever easy.

II ACKNOWLEDGEMENTS

This thesis would not have been possible without the contribution, dedication and support of a number of people and I would like to take a moment to give much deserved thanks to these people.

First and foremost, I would like to thank Jo McNamara for donating her time both supervising and guiding me throughout the project, including staying back after hours. Her dedication, attention to detail and vast knowledge will be an invaluable example to me throughout the rest of my career. I would also like to thank Kirbie Sloan and Stephen Dowdell for donating their time and guidance when I required it and being so willing to take a moment from their busy days to help me with any problem, big or small.

I would particularly like to thank Adrian Rinks and the other staff at Shoalhaven Cancer Care Centre for allowing me access to their equipment to complete this thesis.

Thank you to my academic supervisors, Dr Dean Cutajar and Prof Pete Metcalfe for so patiently working with me; especially through the difficulties I faced changing projects. Knowing you were only an email away gave me confidence that everything would be done right. Your knowledge and passion were inspiring and motivating throughout this thesis.

Lastly, I'd like to thank Mum and Dad, not just for giving me somewhere to live for the past 12 months or for putting up with the stressful times. But for being role models who gave me the freedom to choose my passion and the strength of character to make it a reality. You both showed me that with enough work anything was possible and you being there whenever and for whatever enabled me to have the confidence to tackle this project head on.

III TABLE OF CONTENTS

I CERTIFICATION 1

II ACKNOWLEDGEMENTS 3

III TABLE OF CONTENTS 4

IV LIST OF EQUATIONS 8

V LIST OF FIGURES 10

VI LIST OF TABLES 12

VII ABSTRACT 13

VIII LIST OF ABBREVIATIONS 14

1. INTRODUCTION 1

1.1 Radiotherapy 1

1.2 Treatment Planning 1

1.3 Dosimetry 2

1.4 Thesis Aims 4

1.5 Overview of Thesis 5

2. LITERATURE REVIEW 6

2.1 Interactions of Photons with Matter 6

2.1.1 Attenuation coefficients 7

2.1.2 Atomic Number 9

2.1.3 The Photoelectric Effect 11

2.1.4 Incoherent Scattering – The Compton Effect 13

2.1.5 Pair Production 15

2.1.6 Coherent (Rayleigh) Scattering 16

2.1.7 Bremsstrahlung 16

2.2 Passive *in vivo* dosimeters 18

2.2.1 Optically Stimulated Luminescent Dosimeters 18
2.2.2 Thermoluminescent Dosimeters 20
2.2.3 Radiophotoluminescent Glass Dosimeters 24
2.2.4 Radiation sensitive film 24
2.2.5 Radiation sensitive gels 26
2.3 Real-time *in vivo* Dosimeters 27

2.3.1 Ionisation Chambers 27
2.3.2 Diamond Dosimeters 28
2.3.3 Metal Oxide Semiconductor Field Effect Transistor Dosimeters 28
2.3.4 Dosimetry using Electronic Portal Imaging Devices 30
2.4 Properties of Clinical Dosimeters 30

2.4.1 Fading 30
2.4.2 Sensitivity 31
2.4.3 Angular Dependence 32
2.4.4 Energy Dependence 33
2.4.5 Tissue Equivalence 33
3. EXPERIMENTAL INVESTIGATION 34
3.1 Introduction and Materials 34

3.2 Preliminary Investigation - Annealing Tests 36

3.2.1 Aim 36
3.2.2 Materials and Method 37
3.2.3 Results 38
3.2.4 Discussion 41
3.3 Preliminary Investigation - Batch Sensitivity 41

3.3.1 Aim 42
3.3.2 Materials and Method 42
3.3.3 Results 43
3.3.4 Discussion 45
4. DOSIMETER PROPERTIES 47

4.1 Short Term Fading 47

4.1.1 Introduction 47
4.1.2 Aim 47
4.1.3 Materials and Method 48
4.1.4 Results 49
4.1.5 Discussion 49

4.2 Signal Loss Per Readout 51

4.2.1 Introduction 51
4.2.2 Aim 51
4.2.3 Materials and Method 51
4.2.4 Results 52
4.2.5 Discussion 52

4.3 Reproducibility 54

4.3.1 Introduction 54
4.3.2 Aim 54
4.3.3 Materials and Method 54
4.3.4 Results 56
4.3.5 Discussion 58

4.4 Dose Linearity 59

4.4.1 Introduction 59
4.4.2 Aim 59
4.4.3 Materials and Method 59
4.4.4 Results 60
4.4.5 Discussion 60

4.5 Dose Rate Dependence 61

4.5.1 Introduction 61
4.5.2 Aim 61
4.5.3 Materials and Method 61
4.5.4 Results 62
4.5.5 Discussion 62

4.6 Angular Dependence 64

4.6.1 Introduction 64

4.6.2 Aim 64

4.6.3 Materials and Method 64

4.6.4 Results 67

4.6.5 Discussion 67

4.7 Depth Dose Curve 68

4.6.6 Introduction 68

4.6.7 Aim 68

4.6.8 Materials and Method 68

4.6.9 Results 70

4.6.10 Discussion 71

5. MEPITEL® FILM 73

5.1 Effect of Mepitel® Film on surface dose 73

5.1.1 Introduction 73

5.1.2 Aim 75

5.1.3 Materials and Method 75

5.1.4 Results 75

5.1.5 Discussion 76

6. CONCLUSION 77

7. REFERENCES 79

IV LIST OF EQUATIONS

Equation 1: The Beer-Lambert law of light absorption 7

Equation 2: Relative magnitude of attenuation coefficients 8

Equation 3: Expressions for mass energy transfer coefficient 8

Equation 4: Relationship between mass energy transfer coefficient and mass energy absorption coefficient 9

Equation 5: Determination of effective atomic number 9

Equation 6: Total Photon interaction cross section 10

Equation 7: Calculation of effective atomic number 10

Equation 8: Photoelectric interaction cross-sections 11

Equation 9: Kinetic energy of Photoelectron 12

Equation 10: Compton conservation of energy and momentum 13

Equation 11: Angular dependent form of Compton Scatter Equation, where h is Planck's constant, v is frequency, p is linear momentum and c is speed of light in ms^{-1} 13

Equation 12: Compton relationship of photon wavelength 13

Equation 13: Compton interaction equation 14

Equation 14: Klein-Nishina formula for scattering cross section 14

Equation 15: Atomic cross section of Rayleigh scattering 16

Equation 16: Fraction of energy loss by Bremsstrahlung to total energy loss 17

Equation 17: Relation of signal Intensity to temperature for LiF:Mg,Ti TLD 22

Equation 18: Optical Density (OD) where I_0 is light intensity without film and I is intensity with film present 25

Equation 19: Homogeneous dosimeter energy dependence 33

Equation 20: Relation between Standard Deviation (σ), average (< >) of values (x) and total number of values (n) [5] 37

Equation 21: Derivation of 95% confidence interval used in error expression [5] 38

Equation 22: Decay function of dosimeter 645 84M 53

Equation 23: Decay function of dosimeter 647 45I 53

Equation 24: Decay function of dosimeter 647 26K 53

Equation 25: Decay function of dosimeter 645 19J 53

Equation 26: Decay function of dosimeter 047 33W 53

Equation 27: Average Rate of signal loss per readout 53

Equation 28: Correction factor, k, for ionisation chambers 55

Equation 29: Relation between Optical Density (OD) and Dose for Calibration Curve 71

V LIST OF FIGURES

Figure 1: Energy and Z dependence of photon interactions [5] 6

Figure 2: Mass attenuation coefficients, total attenuation and total absorption [14] 7

Figure 3: Variation of effective atomic number from 10keV-100GeV [20] 11

Figure 4: Photoelectric effect (Adapted from Fig 5.5) [22] 12

Figure 5: Illustration of the Compton Effect. Adapted from Kahn [22] 14

Figure 6: Pair production process. Adapted from Kahn [22] 15

Figure 7: Schematic of mechanism of OSL interaction [28] 18

Figure 8: Typical LiF:Mg,Ti glow curve, showing the individual peaks. Peak 6 is omitted [37] 22

Figure 9: Properties of clinically useful TL dosimeters. Adapted from Mayles, Nahum and Rosenwald [10] 23

Figure 10: Standard 0.6cc Farmer Ionisation Chamber [22] 28

Figure 11: Schematic of MOSFET dosimeter [52] 29

Figure 12: Graph of fading of Al_2O_3:C OSLDs over time [35] 31

Figure 13: Loss of sensitivity of OSL through multiple readings [56] 32

Figure 14: Landauer InLight microStar OSL readout system 34

Figure 15: Gammasonics® OSL manual annealing lighbox 36

Figure 16: Background dose trend after repeated use (95% confidence interval) 41

Figure 17: Arrangement of OSLs in grid positioned in beam field (shown in yellow) 43

Figure 18: 6 MV Batch Sensitivity Averages 44

Figure 19: 10 MV Batch Sensitivity Averages 45

Figure 20: Variation in sensitivity at 6 & 10MV for each dosimeter (%) (95% conf. int. not visible) 45

Figure 21: Experimental setup for 6 MV Short term fading 48

Figure 22: 6 MV Short Term Fading results with 95% confidence interval 49

Figure 23: Signal loss per readout for 5 dosimeters 52

Figure 24: Reproducibility Setup 55

Figure 25: Dosimeter 64549G variation over 10 readouts 56

Figure 26: Dosimeter 64724O variation over 10 readouts 56

Figure 27: Dosimeter 57183U variation over 10 readouts 57

Figure 28: 0.6cc Farmer Ionisation chamber variation over 10 readouts 57

Figure 29: OSLD and 0.6cc Farmer Ionisation chamber linearity up to 800MU (Maximum error 0.026%) 60

Figure 30: Dose rate dependence 62

Figure 31: OBI image of steel fiducial in Perspex cylinder 65

Figure 32: Angular Dependence Jig (The University of Wollongong) 65

Figure 33: Angular Dependence Setup 66

Figure 34: Angular Dependence of OSLDs 67

Figure 35: Depth Dose Setup 69

Figure 36: Sheet of EBT3 with 3cm grid marked out 70

Figure 37: EBT3 Radiochromic film calibration curve (Maximum error 1%) 70

Figure 38: OSL, EBT3 and Attix Ion Chamber normalised depth dose at 6MV (95% conf. int. not visible) 71

Figure 39: Build up effect of Mepitel® Film measured using OSL and Attix Ionisation Chamber (95% conf. int. shown) 75

VI LIST OF TABLES

Table 1: Initial OSL annealing results 38

Table 2: 12hr anneal of used dosimeters..... 39

Table 3: Initial and Final dose of 24hr anneal 40

Table 4: Relation between dosimeter and grid position during sensitivity measurement 43

VII ABSTRACT

Al_2O_3:C has increasingly been used for optically stimulated luminescence (OSL) dosimetry, initially for personal dosimeters and more recently through the Landauer commercial OSL system for dosimetry. The system couples the InLight® microStar reader with NanoDot® dosimeters that were then paired with a GammaSonics® manual annealing lightbox to perform robust, simple and reliable dosimetry.

Using this system, an extensive list of properties relevant to NanoDot® use in a clinical environment was determined. These include: thorough annealing using this setup requires dosimeters to be in the lightbox for 36hrs; batch sensitivities were determined for 6 and 10 MV to be between 1.038 and 0.963 with little difference in values seen between energies; 20% fading was observed in the initial 30 minutes following exposure with stable readings for the next 48 hrs; 0.05% signal loss was observed per readout, indicating a large number of readouts are possible before statistically significant dose loss; dose reproducibility was found to be 4.17 ± 0.998% (2SD); linearity was observed from 0-500cGy with supralinearity observed beyond 500cGy; 5% dose rate dependence was observed between 100MU/min and 600MU/min; ±4% angular dependence was observed across the range of 360^{o}; NanoDots® were found to over respond by 164% compared to EBT3 film at the surface.

NanoDots® were used to investigate the dose build up effect of Mepital® film when applied for moist desquamation and erythema prevention. Whilst it was found that the presence of film did increase the surface dose, an accurate value could not be determined using OSL, however Attix chamber investigation determined this effect to be 25.68% at 6 MV and 19.42% at 10 MV. Overall, it is expected that NanoDots® provide a useable alternative dosimetry method and could be used clinically.

VIII LIST OF ABBREVIATIONS

Al_2O_3:C	Carbon doped Aluminium Oxide
Co-60	Cobalt 60, radioactive isotope of Cobalt
CPU	Central Processing Unit
CT	Computed Tomography
CVD	Chemical Vapour Deposition
d_{max}	Depth at which maximum dose is delivered
DVH	Dose Volume Histogram
EPID	Electronic Portal Imaging Device
GDP	Gross Domestic Product
IAEA	International Atomic Energy Agency
ICRU	International Comission on Radiation Units and Measurements
IMRT	Intensity Modified Radiation Therapy
LET	Linear Energy Transfer
LiF	Lithium Fluoride
Linac	Linear Accelerator
MOSFET	Metal Oxide Semiconductor Field Effect Transistor Dosimeter
NTCP	Normal Tissue Complication Probability
OBI	On Board Imager
OD	Optical Density
OSL	Optically Stimulated Luminescence
OSLDs	Optically Stimulated Luminescent Dosimeters
PDD	Percentage Depth Dose
RPLDs	Radiophotoluminescent glass dosimeters
RSG	Radiation Sensitive Gels
SSD	Source to surface distance
TCP	Tumour Control Probability
TLD	Thermoluminescent Dosimetry
UV	Light in the ultraviolet range of spectrum
VMAT	Volume Modulated Arc Therapy

1. INTRODUCTION

1.1 Radiotherapy

As one of the primary treatment methods of Australia's leading cause of death, radiotherapy is a critical technology to the medical field as a whole. With 326,600 people (or approximately 1.5% of the total population) having cancer at the time of the last health census, [1] improvement in the fields of radiotherapy treatment delivery and patient comfort have the possibility of directly or indirectly improving the lives of a large number of people.

One of the appeals of cancer treatment by radiotherapy is the amount of understanding of the interaction of radiation with tissue. Since the discovery of the X-ray by Wilhelm Rontgen on the 8th of November 1895 [2], study has continued on the interaction of radiation with tissue. Radiation induced generation of free radicals and their toxicity to cancerous tissue, as well as a sound understanding of the radiosensitivity of each tissue type (see ICRP 103 [3]), enable radiation oncologists, therapists and physicists to deliver a treatment with maximum TCP and minimal NTCP. Additionally, the wide variety of radiotherapy delivery modalities such as: VMAT, IMRT, IMAT, Brachytherapy and more, give clinical staff a range of options to limit the exposure of normal tissue. [4]

1.2 Treatment Planning

As a treatment modality, the primary goal of radiotherapy is to deliver a lethal dose to the tumour while minimising dose to the surrounding healthy tissue. To this end, each treatment delivery is highly personalised and extensively planned prior to delivery. Understanding the physical processes involved in radiation interaction with tissue allows medical physicists and radiation therapists to effectively deliver a radiotherapy regimen set out by a medical professional, however, a large number of variables make effective treatment planning an exceedingly difficult task.

The ICRU 50 report is an extremely important document in the standardisation of photon beam delivery. ICRU 50 provides guidance in the prescription, recording and reporting of photon therapy by outlining and defining quantities and terms used in treatment. The report recommends a general dose uniformity of +7% and -5%, however these numbers are designed to be used as a guide [5]. Often, radiotherapy treatments include one or more "critical structures" or organs at risk. These are regions in or adjacent to the beam path with high sensitivity to radiation, such as the eye in nasopharyngeal treatments or the rectum in prostate treatment. A list of critical structures can be found in ICRU 50 and 62, however this cannot be considered comprehensive and critical structures need to be considered based on treatment type and patient status [5].

Due to the nature of critical structures, dose to these areas needs to be carefully considered in the treatment planning phase. For rigorousness however, it is common to monitor critical structures with an appropriate dosimeter throughout treatment delivery.

1.3 Dosimetry

Dosimetry is defined by Dorland's Medical Dictionary for Health Consumers Elsevier [6] as:

"Scientific determination of the amount, rate, and distribution of radiation emitted from a source of ionizing radiation, in *biological definition*, measuring the radiation induced changes in a body or organism, and in *physical definition*, measuring the levels of radiation directly with instruments."

This definition shows the broad nature of dosimetry as a field and the importance of accurate dosimetry in a large number of medical and industrial tasks. In the context of radiotherapy however, there exists two steps in which dosimetry plays a critical role. The first is during the treatment planning phase, the role of which has been discussed; the

second is the *in vivo* dosimetry during treatment delivery, in which OSLDs will primarily be used.

The motivation for *in vivo* dosimetry is complex but is best summarised in Metcalfe, Kron and Hoban [7]:

i. Increasing complexity of equipment providing more room for error
ii. Increasing difficulty of treatment techniques such as gating, VMAT and IMRT
iii. Tighter dose rationale due to improvement in the understanding of both the target tissues and the biological effects of ionising radiation
iv. More thorough follow up and less "routine" side effects make identification of side effects and secondary tumours more likely.
v. Increased emphasis on liability and an ever more litigious culture means a thorough and accurate record of dose distribution during treatment is an important part of hospital protection.

Current radiotherapy dosimetry is complex to discuss due to the most suitable dosimeter for a measurement not always being the same. Instead, it is up to the physicist to determine the best dosimeter on a case-by-case basis. Despite this, there are a number of dosimeters which are widely used. These include a number of ionisation chambers (such as Thimble, Parallel Plate and Farmer), radiation sensitive film (EBT-2 and EBT-3), MOSFET semiconductor dosimeters, as well as diamond, gel, alanine and plastic scintillation dosimeters. Each has a unique set of advantages and disadvantages, making them appropriate for certain situations. [5, 8-10]

The final type of dosimeter is luminescence based dosimetry, both thermoluminescent and optically stimulated luminescent. The first type, thermoluminescent dosimetry, requires

careful handling, preparation and readout to use heating to release photons that are proportional to a dose of radiation.

The second type, Optically Stimulated Luminescent (OSL) dosimetry uses robust detectors with extremely quick and simple preparation and readout procedures. As with Thermoluminescent Dosimeters (TLDs), OSL dosimetry uses release of photons proportional to dose as a measurement method. Unlike TLD however, OSL dosimetry uses lasers to stimulate release of these photons instead of heat. OSL dosimeters themselves have different properties depending on the crystal from which they are manufactured. Although Al_2O_3:C (Carbon doped aluminium oxide) is the most clinically prevalent, a variety of other materials which exhibit OSL are used, including but not limited to, terbium dosed fluoride-phosphate glass as well as crystals of LiF and BeO. [5, 11-13]

1.4 Thesis Aims

The research goals are to provide an accurate and comprehensive reference of the properties and use of NanoDot® OSLDs. This will be achieved by:

i. A thorough breakdown of dosimeter properties important for clinical dosimetry.
ii. Initial investigation into clinical use of a NanoDot® OSL system including annealing time and time before readout.
iii. Calculation of each clinically important property through careful experimentation.
iv. Recommendation on the magnitude of important dose response properties
v. Demonstration of use of NanoDot® OSLDs being used clinically for investigation of Mepitel® film.

1.5 Overview of Thesis

Chapter 1 introduces the focus areas of the thesis and a brief explanation of the significance of these areas, both to the thesis and medical physics as a whole. Radiotherapy, treatment planning and dosimetry are each outlined to provide the reader with an understanding of the fields affected by this work. In addition to this the aims and outcome of this thesis are stated.

Chapter 2 contains a thorough literature review; this is designed to be a self-contained background resource explaining basic interactions of radiation with matter, common detector types and uses as well as important properties of clinical radiotherapy dosimeters.

Chapters 3, 4 and 5 contain the original research components of the thesis. Chapter 3 covers initial experiments relating to the day to day use of OSLDs. Chapter 4 systematically covers the aim, materials, method, results and discussion of the relevant detector properties. This is done through a series of sub chapters with each covering one property important to understand for safe use of OSLDs. Chapter 5 introduces Mepitel® film and a chapter covering research conducted into the effect of using Mepitel® film on the dose distribution.

Chapter 6 summarises the overall findings of the research as well as relevant conclusions and possible future research prospects. This includes recommendations on the clinical use of NanoDot® OSLDs.

2. LITERATURE REVIEW

2.1 Interactions of Photons with Matter

The basis of all radiotherapy treatments is the transfer of energy from the radiation beam to the target volume, whilst sparing the surrounding healthy tissue as much as possible. Photons interact with matter in a number of different ways, depending on the composition of the material and the energy of the photons. Figure 1 summarises the energies of predominance for the three most clinically significant mechanisms of interaction; the Photoelectric Effect, the Compton Effect and Pair Production [5].

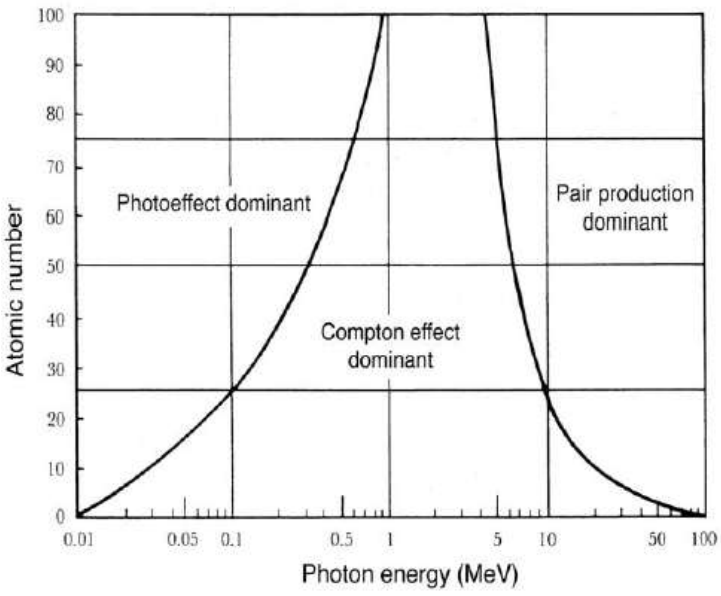

Figure 1: Energy and Z dependence of photon interactions [5]

Figure 2 from Evans [14] shows the total contribution of each interaction to the total absorption in air from the Photoelectric and Compton Effects as well as Pair production. The total attenuation is also shown, which includes Rayleigh scattering.

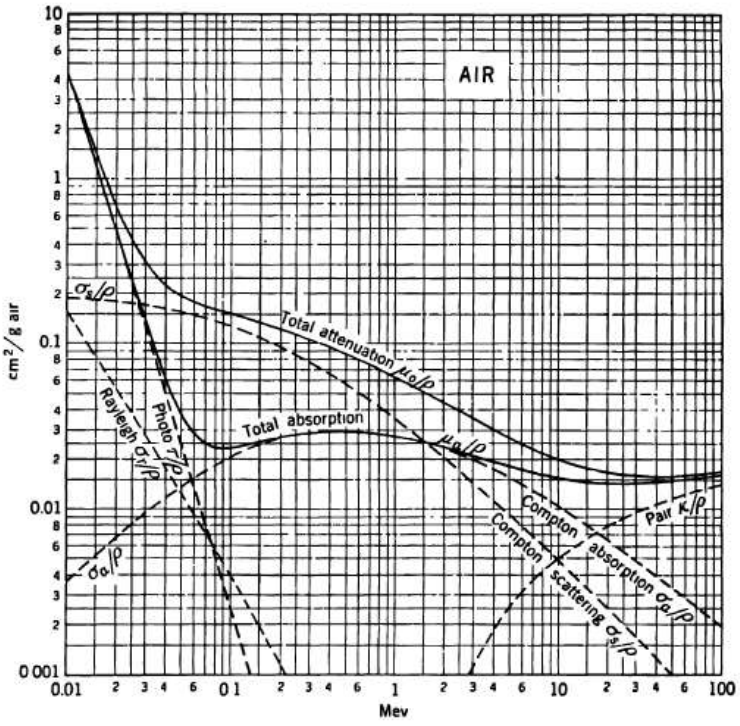

Figure 2: Mass attenuation coefficients, total attenuation and total absorption [14]

2.1.1 Attenuation coefficients

Unlike electrons and other charged particles, photons do not continuously lose energy through Coulomb-force interactions, instead depositing most or all of their energy in a single interaction event. A number of similar but distinct quantities exist when talking about energy loss of a photon beam, the first of which is the probability that a photon will interact for a given path length, called the linear attenuation coefficient. The fraction of N_0 particles lost over a unit dx is given in Equation 1, which gives a differential expression which integrated over a path length x gives the second expression, known as the Beer-Lambert Law:

$$\frac{dN_0}{N_0} = -\mu dx \tag{1}$$

$$\frac{N}{N_0} = e^{-\mu x}$$

Equation 1: The Beer-Lambert law of light absorption

The mechanism of loss gives rise to two other attenuation coefficients, the linear energy transfer coefficient (μ_{tr}) which is a measure of the energy lost and the linear energy absorption coefficient (μ_{ab}) which is a measure of the energy *deposited* in a material. Note that the energy transferred and the energy deposited are not the same, as shown in Equation 2: [7]

$$\mu < \mu_{tr} < \mu_{ab} \tag{2}$$

Equation 2: Relative magnitude of attenuation coefficients

The linear attenuation coefficient characterises changes in the beam, but neglects the attenuating material. Since the composition of a material will affect the attenuation per unit path length, the linear attenuation coefficient is divided by the density to give a density independent quantity, the mass attenuation coefficient (μ/ρ).

Similarly to the linear attenuation case, the mass attenuation coefficient deals with total loss per path length. The mass energy transfer coefficient represents the energy transfer per unit path length, which although not widely used, is given in Equation 3: [7, 15]

$$\frac{\mu_{tr}}{\rho} = \frac{\tau_{tr}}{\rho} + \frac{\sigma_{tr}}{\rho} + \frac{\kappa_{tr}}{\rho} \tag{3}$$

$$\mu_{tr} = \mu(\frac{\overline{E_{tr}}}{E})$$

Equation 3: Expressions for mass energy transfer coefficient

In Equation 3, note that the overall mass energy transfer coefficient ($\frac{\mu_{tr}}{\rho}$) is the sum of the contribution each photon interaction (photoelectric ($\frac{\tau_{tr}}{\rho}$), compton ($\frac{\sigma_{tr}}{\rho}$), and pair production ($\frac{\kappa_{tr}}{\rho}$)). The second expression gives the energy transfer coefficient (μ_{tr}) which includes the average energy transferred into kinetic energy of particles per interaction, denoted E_{tr}.

Possibly the most useful quantity for discussion of photon interactions with matter is the mass energy absorption coefficient. Like the linear absorption coefficient, this is a measure of the energy deposited in a material through the interactions of photon with matter discussed in 2.1.3, 2.1.4 and 2.1.5. The relationship between the mass energy transfer coefficient and the mass energy absorption coefficient is shown here, where g is the average fraction of energy not deposited to orbital electrons such as by bremsstrahlung and positron annihilation. Note that all mass absorption coefficients have SI units of m^2kg^{-1}. [15]

$$\frac{\mu_{en}}{\rho} = \frac{\mu_{tr}}{\rho}(1-g) \tag{4}$$

Equation 4: Relationship between mass energy transfer coefficient and mass energy absorption coefficient

Although calculation of mass energy absorption coefficients is difficult, extensive tables exist both online and in appendices of various textbooks. For comprehensive lists of mass attenuation coefficients, as well as further explanation of terms, see Attix [15] and NIST [16].

2.1.2 Atomic Number

Figure 1 shows the dependence of interaction dominance against both photon energy and atomic number. This provides a simple comparison for single elements; the body composition varies drastically and is never a single element. As such, effective atomic number is used (Z_{eff}) to provide a representation of the atomic number of the tissue for calculations.

The historic calculation of Z_{eff} used comes from Mayneord [17] and is given as:

$$Z_{eff} = (a_1 Z_1^{2.94} + a_1 Z_1^{2.94} + a_1 Z_1^{2.94} + \cdots a_1 Z_1^{2.94})^{\frac{1}{2.94}} \tag{5}$$

Equation 5: Determination of effective atomic number

However this simplistic form is described by Taylor [18] as a questionable approach, therefore it is only referred to in passing in contemporary literature. [19, 20]

Equation 7 is just one of a variety used throughout the literature for determination of a more rigorous Z_{eff} value using the total interaction cross section. The total photon cross section is given by Equation 6, from which it can be seen that the total cross section is a summation of the contributions of each interaction discussed above and σ_p, where $\sigma_p$is photonuclear cross section. These values themselves however are functions of mass attenuation coefficients, atomic and molecular weights as well as total number of molecules, resulting in an extremely intricate calculation. [20]

$$\sigma = \sigma_c + \sigma_{in} + \tau + \kappa + \sigma_p \tag{6}$$

Equation 6: Total Photon interaction cross section

$$Z_{eff} = \frac{\sigma_a}{\sigma_e} \tag{7}$$

Where:

$$\sigma_e = (\frac{1}{N}) \sum_i \left\{ (\frac{f_i A_i}{Z_i})(\frac{\mu}{\rho})_i \right\}$$

And,

$$\sigma_a = \frac{(\frac{1}{N})(\frac{\mu}{\rho})_{bio} \sum_i n_i A_i}{\sum_i n_i}$$

Equation 7: Calculation of effective atomic number

As well as the probability of different photon interactions changing with energy, the effective atomic number can also vary. Extensive investigation has been done into graphing the variation of effective Z across energy ranges due to its implications for radiotherapy [18, 21]. Figure 3 shows effective atomic number measurements for 8 important human tissues across 10keV-100GeV.

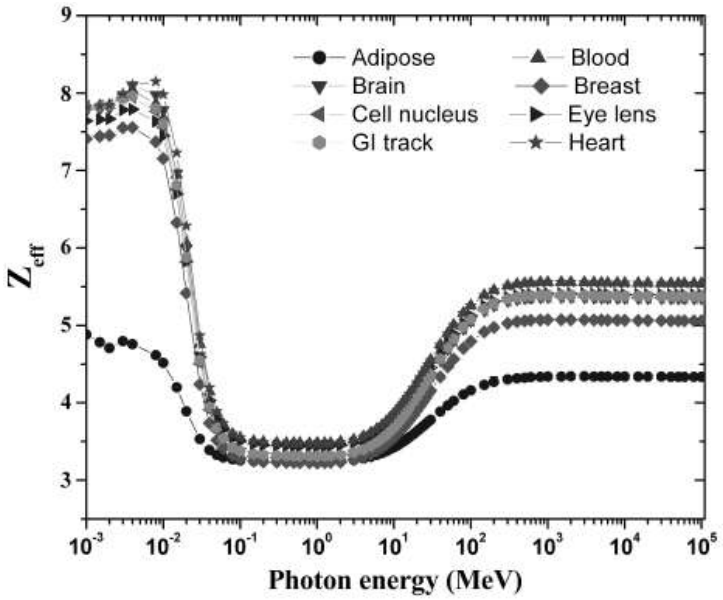

Figure 3: Variation of effective atomic number from 10keV-100GeV [20]

2.1.3 The Photoelectric Effect

The Photoelectric effect is the most probable method of interaction in low energy radiology such as Orthovoltage treatments. As shown in Figure 1, the cross section of interaction varies both with photon energy and atomic number while the Z of tissue is low and the energy of typical radiotherapy treatments being reasonably high. The cross section of this interaction is given in Equation 8. Although a number of variations are quoted in text the most common is given here: [22]

$$\frac{\tau}{\rho} \propto \frac{Z^3}{h\nu^3} \tag{8}$$

Equation 8: Photoelectric interaction cross-sections

The form used by Kahn is commonly referenced [8, 15] as this is the most practical approximation for high Z materials at low energy where the photoelectric effect is dominant.

The ratio given in differs from the mass attenuation coefficient (μ/ρ) discussed earlier as it is the photoelectric attenuation coefficient, rather than the mass attenuation coefficient.

The photoelectric effect involves the transfer of a photon's entire energy to a bound electron in an atoms inner K, L, M and N shells. The direction of the ejected electron depends on the angle and momentum of the incident photon. The ejected electron creates a vacancy in one of the inner shells and another electron drops from a higher shell to occupy this vacancy. The process of the electron filling this vacancy releases characteristic X-ray photons with a probability of releasing Auger electrons due to self-absorption of these X-rays. This process is summarised in Figure 4 [15, 22].

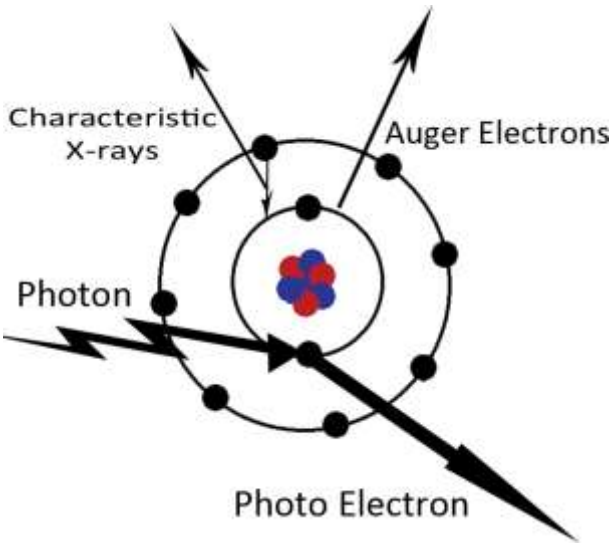

Figure 4: Photoelectric effect (Adapted from Fig 5.5) [22]

Given initial photon energy of hν interacting with a shell of bounding energy E_b the kinetic energy of the ejected photoelectron can be given in Equation 9: [15]

$$T = h\nu - E_b - T_a \tag{9}$$

Equation 9: Kinetic energy of Photoelectron

Typically, the T_a is neglected as the kinetic energy given to the atom is approximately zero; however, it is included here for completeness. The photoelectron is ejected from the atom at a spectrum of angles depending on the momentum and angle of the incident electron.

2.1.4 Incoherent Scattering – The Compton Effect

Unlike the photoelectric effect, the process of incoherent scattering (referred to as the Compton Effect) is extremely important for most modern radiotherapy treatments. Unlike the Photoelectric effect, the Compton Effect is "the only interaction of importance from 200keV to 2MeV" [7] for low Z materials such as tissue. Given its clinical importance and relevance, the Compton Effect will be discussed in detail, more detail may be obtained in [15, 23, 24].

The interaction between the photon and the isolated atomic electron causes a change in the energy and momentum of both the electron and the photon as given in Equation 10 and 11 and illustrated in Figure 5: [15]

$$E = h\upsilon - h\upsilon' \tag{10}$$

Equation 10: Compton conservation of energy and momentum

$$h\upsilon = h\upsilon' \cos\phi + pc\cos\theta \tag{11}$$

Equation 11: Angular dependent form of Compton Scatter Equation, where h is Planck's constant, v is frequency, p is linear momentum and c is speed of light in ms^{-1}

This changing energy causes an associated change in wavelength according to the Planck equation which is given in Equation 12: [5]

$$\Delta\lambda = \lambda_C(1 - \cos\theta) \tag{12}$$

Equation 12: Compton relationship of photon wavelength

From these conditions it is possible to derive the well-known Compton equation relating the energy of the scattered photon, the initial photon and the electron. This is given in Equation 13 where m_0c^2 is the rest-mass energy of the electron (0.511MeV). [15]

$$h\upsilon' = \frac{h\upsilon}{1 + \frac{h\upsilon}{m_0 c^2}(1 - \cos\theta)} \tag{13}$$

Equation 13: Compton interaction equation

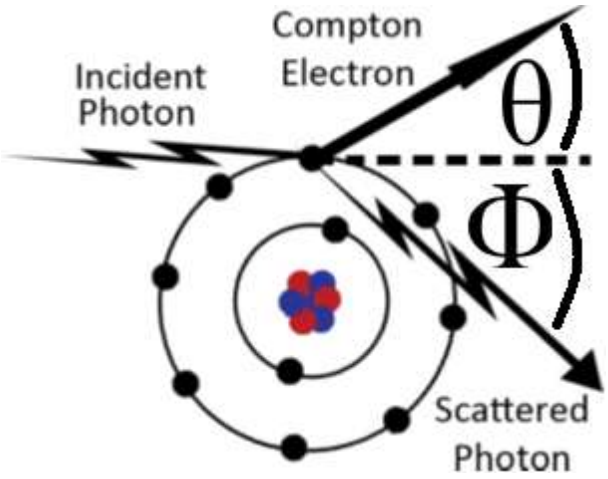

Figure 5: Illustration of the Compton Effect. Adapted from Kahn [22]

The angle of the scattered photon is a useful quantity predicted by the differential scattering cross section, given by the Klein-Nishina formula shown here as , where r_0 is the radius of the electron and $\alpha \equiv h\upsilon m_0 c^2$: [8]

$$\frac{d\sigma}{d\Omega} = Zr_0^2\left(\frac{1}{1 + \alpha(1 - \cos\theta)}\right)^2\left(\frac{1 + \cos^2\theta}{2}\right)\left(1 + \frac{\alpha^2(1 - \cos\theta)^2}{(1 + \cos^2\theta)[1 + \alpha(1 - \cos\theta)]}\right) \tag{14}$$

Equation 14: Klein-Nishina formula for scattering cross section

The minimum and maximum energy transfers occur with photon scattering angles of 0^{o} and 180^{o} respectively, with the energy transferred to the electron being 0 and $E_{max} = h\nu\frac{\alpha}{1+2\alpha}$ in each case.

2.1.5 Pair Production

The third primary photon interaction, pair production, involves the spontaneous generation of an electron positron pair due to the energy mass equivalence. At the end of its range, the positron recombines with an electron to produce two 0.511MeV photons. These photons are ejected in opposite directions perpendicular to the propagation of the positron to conserve momentum. Figure 6 illustrates the generation of the electron-positron pair with the annihilation occurring outside the diagram [22].

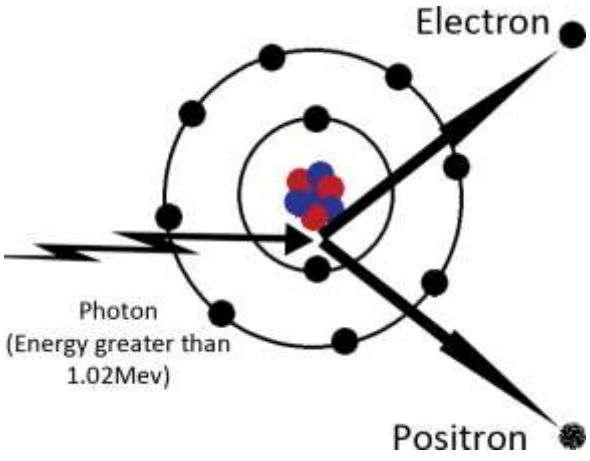

Figure 6: Pair production process. Adapted from Kahn [22]

The rest masses of both an electron and positron are 0.511MeV; which provides a threshold for pair production to occur of $2 \times 0.511\text{MeV} = 1.022\text{MeV}$. Any photons below this energy will not cause pair production and any energy above this will be given as kinetic energy after generation. Due to the relatively low energy of radiotherapy treatment, pair production is not a clinically significant interaction for treatment. However, it is important in PET imaging used for treatment planning. [8].

2.1.6 Coherent (Rayleigh) Scattering

Although not contributing to the energy transfer coefficient, Rayleigh scattering contributes to the attenuation coefficient. Unlike the Compton Effect, Rayleigh scattering occurs between a photon and a bound electron, meaning the interaction affects the entire atom. Rayleigh scattering is elastic in that the photon loses basically no energy, but is slightly deflected and the atom shifts enough to conserve momentum. Although occurring at all energies, the deflections are small and decrease with increasing energy. The interaction causes no transfer of energy and as such does not directly contribute to dose or kerma.

The cross section for Rayleigh scattering is given in Equation 15 and like other photon interactions depends both on the energy of the photon and the atomic number, where k is a constant of proportionality and the units are cm^2g^{-1}. [15]

$$\frac{\sigma_R}{\rho} = k\frac{Z^2}{(h\nu)^2} \quad (15)$$

Equation 15: Atomic cross section of Rayleigh scattering

2.1.7 Bremsstrahlung

Although primarily significant in generation of clinical X-ray beams, the process of Bremsstrahlung is included here as important background information. For further reading on the production of radiation by Bremsstrahlung, further information may be found in [25, 26].

The deceleration of an electron by interaction with a nucleus causes radiative energy loss in the form of a photon. The maximal energy of this photon cannot exceed the initial energy of the electron due to energy conservation and the closer proximity to the nucleus the greater the energy loss. For an electron beam, this generates a spectrum of radiative energy loss. For a target with minimal scatter and variation in stopping power, the fraction of energy loss

through Bremsstrahlung is given by Equation 15. E_e is the energy of the electron in MeV and n is a material specific energy dependent value, which for Tungsten (a common target for X-ray production) is 649 at 1MeV. [15]

$$\frac{(\frac{dE_e}{\rho dx})_r}{(\frac{dE_e}{\rho dx})} = \frac{E_e Z}{n + E_e Z} \tag{16}$$

Equation 16: Fraction of energy loss by Bremsstrahlung to total energy loss

In vivo dosimeters are separated into two categories depending on the method of operation: passive and active (real time) dosimeters.

2.2 Passive *in vivo* dosimeters

Passive dosimeters accumulate dose over time and upon readout the signal intensity is proportional to the radiation exposure.

2.2.1 Optically Stimulated Luminescent Dosimeters

Optically stimulated luminescence (OSL) refers to the process by which electrons are freed from a semiconducting material through exposure to light. OSL has a number of applications, both for clinical dosimetry and for geological investigations such as dating i.e. estimating the age of a sample. When applied to clinical dosimetry, OSL dosimeters (OSLDs) are particularly useful due to their good tissue equivalence, insensitivity to mechanical and thermal changes and stable radiation sensitivity [27]. Figure 7 illustrates the mechanism of OSL where the traps between the conduction and valence bands are produced by doping a pure semiconducting material with small amounts of impurities.

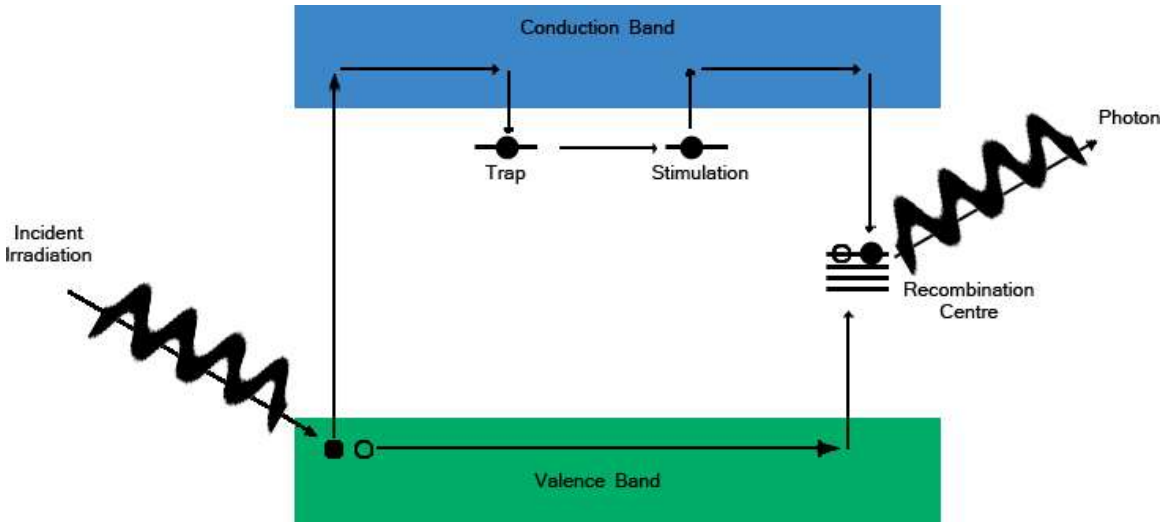

Figure 7: Schematic of mechanism of OSL interaction [28]

A variety of materials exhibit OSL and investigation into each is ongoing, some materials which have been examined for use in clinical dosimetry include CaS:Ce,Sm, Al2O3:C [29], CaF2:Tm [30] and BeO [12] as well as a variety of others. Pingqiang et al. found that up to 5Gy/s for a total dose of 10Gy delivered to CaS:Ce,Sm OSLDs no dose-rate effect was shown on output. Similar results were found for Al2O3:C "influencing factors such as beam quality, dose rate, field size and irradiation temperature did not affect the OSLD response by more than 1%" [31].

LiF OSLDs were found to accurately measure from <1Gy to up to 5 X 10^4Gy, such as those doses used in radiation sterilisation. For the BeO dosimeter, doses over 10Gy caused some saturation however, "deviation to linearity is fewer than 5% at 30Gy" [27]. For low doses, it was theorised that using a 405nm diode for readout, the lowest level of detection (LLD) could be reduced below 1μGy. It was noted by Sommer that OSLDs produced from BeO underestimate radiation under 100keV. In addition to this, some self-absorption occurs below 10keV, although build up foils can compensate the change in energy response. However, it has been found that for Al_2O_3:C OSLDs, response can be considered approximately linear up to 50Gy and sublinearity occurs for accumulated doses above 100Gy[30].

The use of OSLDs for dosimetry of proton and heavy ion beams is also being investigated. One of the primary difficulties in proton and heavy ion dosimetry is a result of the variation in the Linear Energy Transfer (LET) along the path length, resulting in variation of the OSL efficiency. It was concluded however that strip readers showed promise in measurement of lateral profiles [30].

Despite the wide variety of materials exhibiting OSL properties, Al_2O_3:C is primarily chosen for clinical dosimetry and will be used in this work. The primary application of these

dosimeters is for use as *in vivo* dosimeters (meaning occurring in a natural setting, usually with reference to a living organism[32]). According to [33], *in vivo* dosimetry includes:

i. Entrance Dose Measurements
ii. Exit Dose Measurements
iii. Transmission Measurements
iv. Intracavity Absorbed Dose Measurements

The primary dosimeters used in this study, are NanoDot® Al_2O_3:C dosimeters, from Landauer. These OSLDs are a 10mm x 10mm x 2mm chip of light tight plastic enclosing a small disc of Al_2O_3:C. This means they can easily and comfortably be secured to the patient, even using multiple dosimeters for radio sensitive areas such as the eye. Unlike many other dosimeters, the readout process is non-destructive and multiple readouts can be taken from one irradiation.

2.2.2 Thermoluminescent Dosimeters

Thermoluminescent detectors (TLDs) have been a common personal for almost 100 years [34]. TLDs are semiconductor based materials, most commonly LiF activated with combinations of Mg, Ti, Cu and P. The physical processes by which radiation interacts with TLD dosimeters is identical to OSL dosimeters. The incident radiation causes electrons to be excited into the conduction band of the semiconductor creating an electron-hole pair. The electron then drops to an intermediate energy level in the forbidden gap created by the doping. When read, energy is given to the electron, allowing it to move to a recombination centre, where it recombines with a hole. This process release photons, the quantity of which is proportional to the initial dose.

The difference between TLD and OSL however is the method of reading; TLD uses heat to cause recombination, whilst OSL uses light (typically a laser of a specific, known, wavelength). For LiF TLD dosimeters, readout is several hundred degrees whilst for Al_2O_3:C the typical wavelength used for readout is approximately 520nm with recombination emission of 420 and 330nm [30, 35]. The primary advantages of TL dosimeters over many other forms of detection include the lack of cables, enabling much more flexible positioning of the detector and the variety of TL materials which match different human tissues [10]. Unlike OSL's however, TL dosimeters are renowned for being time consuming to readout and fiddly to ensure an accurate reading. Clinical radiotherapy departments which have a carefully developed procedure for using TL dosimeters can produce highly accurate readings; however this may require a staff member dedicated almost entirely to the task of maintaining and reading the dosimeters.

One of the primary reasons for complication of readout comes from the intrinsic property of the crystal lattice. As the crystal is heated for readout, some electrons are liberated at lower temperatures whilst some require more heating to liberate. This phenomenon is described as a "glow curve", with a typical LiF:Mg,Ti glow curve shown in Figure 8. The associated equation of this curve can be seen, however, the complexity of this equation makes using it for direct calculation prohibitively difficult. Equation 17 is derived from an assumption of first order kinetics and is applicable for all phosphorescence, the full derivation can be found in Randall and Wilkins (1945) [36].

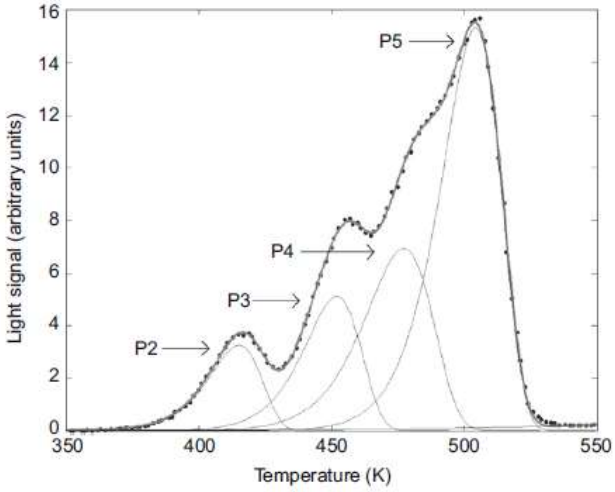

Figure 8: Typical LiF:Mg,Ti glow curve, showing the individual peaks. Peak 6 is omitted [37]

$$I(T) = n_0 s\, e^{(\frac{-E_g}{kT})} e^{\int_0^T (\frac{-s}{R} e^{(\frac{-E_g}{k*T})} dT} \quad (17)$$

Equation 17: Relation of signal Intensity to temperature for LiF:Mg,Ti TLD

A properly set up TL system using LiF:MgTi or LiF:Mg,Cu,P can have a lowest level of detection (LLD) as low as 10 and 1µGy respectively with an error of ±2% [10]. While this would be excellent for use in clinical radiotherapy, a multi institutional study into the clinical use of TLDs found that 22% of users had errors greater than 10%[38]. These two dopings of LiF represent the majority of clinical LiF isotopes with LiF:Mg,Ti being the primary TL material for many years and LiF:Mg,Cu,P being a relatively newer doping first developed in 1978 [38] for its higher sensitivity and more reliable response. The primary readout glow peak of LiF:Mg,Ti occurs at 195^{o}C (peak V) and LiF:Mg,Cu,P occurs at 220^{o}C (peak IV), both glow curves are complex due to the many contributing factors and isolating the relevant peak for readout is the primary challenge in ensuring accurate results. [39, 40]

LiF TLDs have been used extensively throughout medical dosimetry due to their suitable properties, some of these are shown in Figure 9 from Mayles, Nahum and Rosenwald [10].

Dosimetric Properties of Some TL Material

TL Material	Linear Zone (Gy)	Saturation (Gy)	Thermal Fading
LiF:Mg,Ti[a]	5×10^{-5} to 1	10^3	5%-10% per year
LiF:Mg, P, Cu[c]	Up to 12	>40	No Evidence in 100 days
$Li_2B_4O_7$:Mn[a]	10^{-4} to 3	3×10^4	2.5% per month
$Li_2B_4O_7$:Cu[b]	5×10^{-4} to 120	10^3	4% per month
$CaSO_4$:Dy[a]	10^{-6} to 30	10^3	1% to 5% per month
$CaSO_4$:Mn[a]	10^{-7} to 30	10^2	10% per month
CaF_2:Dy[a]	10^{-5} to 10	10^3	25% per month
CaF_2:Mn[a]	10^{-5} to 10	10^3	7% per day

Except $Li_2B_4O_7$:Cu all TLD are distributed by Thermo-Electron (USA)

[a] McKeever (1985)

[b] Wang et al. (1993)

[c] Visocekas et al. (1985)

Figure 9: Properties of clinically useful TL dosimeters. Adapted from Mayles, Nahum and Rosenwald [10]

All TLDs exhibit some form of signal fading which can vary significantly, depending on materials used as well as handling and readout procedures. The values quoted for fading reflect this dependence with no consensus in the literature, however a generally accepted value for LiF:Mg,Ti is <10% per year, for LiF:Mg,Cu,P however, fading is either within experimental uncertainty or not present [37, 38].

Additionally, Figure 11 refers to region of linearity, for many TLDs the region of meaningful results includes some sections of sub- or supra- linearity. This can extend the practically useful dose range orders of magnitude for some TLDs. At extremely low doses ($<5 \times 10^{-5}$Gy) LiF:Mg,Ti exhibits an over response which shows as supralinearity, the same occurs at doses over 1Gy however LiF:Mg,Ti TLDs can be used for readings up to 10^3Gy. In the case of LiF:Mg,Cu,P no supralinearity is observed, instead sublinearity occurs at energies around

150keV. The response of TLDs also changes over time and with use due to the accumulation of radiation damage, affecting the LLD and sensitivity of the detector [38, 41].

LiF dosimeters are found to be both angular and dose rate independent, which removes the need for correction factors in their use as *in vivo* dosimeters. Their availability in multiple forms (rods, powder, ribbons, discs e.t.c) also allows their implementation for a variety of purposes including personal dosimetry, *in vivo* dosimetry and dose mapping.

2.2.3 Radiophotoluminescent Glass Dosimeters

Although first developed in the 1950's, radiophotoluminescent glass dosimeters (RPLDs) have not been widely used [42]. This was primarily due to there being no way to readout RPLDs after low dose exposures; however the development of pulsed UV lasers have enabled much higher sensitivity and accuracy of measurements [43].

RPLDs work by radiation exposure causing the formation of silver ion (Ag^{+} or Ag^{2+}) luminescence centres within silver activated phosphate glass. These luminescence centres exhibit orange wavelength fluorescence when exposed to pulsed UV light. Similarly to OSLDs, the intensity of this fluorescence is related to the initial radiation exposure, however unlike OSLDs, there is no destruction of these luminescence centres in readout [5].

This means that RPLDs theoretically have no signal loss or fading, which combined with low angular dependence, high reproducibility, small size and wide dose range makes them excellent possible future *in vivo* dosimeters [42, 43].

2.2.4 Radiation sensitive film

Two types of film have been used for radiation dosimetry, radiographic and radiochromic film.

Radiographic film; consists of a silver bromide (AgBr) emulsion over a supporting polymer. This emulsion is sensitive to visible light as well as radiation and as such must be handled in darkened conditions prior to exposure. After exposure to radiation, the silver ions form what is termed “sensitivity specks” which vary in size depending on the radiation. These sensitivity specks form the basis of the latent image, which after development of the film, becomes visible. After being developed, radiographic film is fixed to prevent any further sensitivity specks forming and then washed to remove residual emulsion and development chemicals [10, 22, 44].

The silver centres present on the film change its optical density (OD) proportional to the incident radiation, where optical density is defined according to Equation 19: [8]

$$OD = \log_{10}(\frac{I_0}{I}) \tag{18}$$

Equation 18: Optical Density (OD) where I_0 is light intensity without film and I is intensity with film present

Radiochromic film works similarly to radiographic film, however instead of a silver bromate emulsion on a supporting polymer; radiochromic film consists only of a polymer containing a radiation sensitive dye. This has the substantial advantages of making radiochromic film comparatively insensitive to light whilst still being sensitive to gamma, x-ray and UV radiation as well as removing the intricate developing procedure, instead only a flatbed scanner with image analysis software is needed. Although not useable for absolute dosimetry, carefully calibrated radiochromic film can have ±3% precision and is also one of the few dosimetry methods providing a 2D dose map [22, 44].

The use of EBT Grafchromic film for radiotherapy is a result of the improvement of the properties most limiting to the use of other films. The low energy dependence and accuracy of doses below 2Gy are both important features increasing the reliability of EBT film in

radiotherapy applications. A wide variety of Radiochromic film types have been used since their development in the late 1960's including: XR-T, RTQA, XR-RV2, XR-QA. The differences in these films primarily centre on thicknesses and compositions of emulsions and sensitive layers. Variation of these factors changes the nominal dose range, thickness and sensitivity of the films allowing different uses. Whilst some of these films have been superseded, some can still be used today. [45, 46]

The next step in Gafchromic film development was the EBT film with a relatively simple construction, sensitivity to a higher energy and all the desirable properties for use in radiotherapy, multiple iterations of this film have been produced as technology has improved with EBT3 the film currently used.

2.2.5 Radiation sensitive gels

As with radiation sensitive film, radiation sensitive gels (RSGs) undergo a chemical change when exposed to radiation. When exposed to radiation, RSGs undergo radiolysis and vinyl monomers combine to form polymers, often becoming visibly altered in the process.

Despite the visible changes in RSGs, quantification of this can be difficult. MRI is the currently preferred method as the polymerisation process causes significant change in the spin-spin relaxation rate. The inhomogeneities in the external magnetic and radio fields become a source of inaccuracy if other MRI imaging modes are used. In addition to this, X-ray CT is ineffective as the polymerisation process causes a change in Hounsfield number of about 1HU Gy^{-1} [47].

The chemistry of RSGs is complex and not covered here but the primary interest is the formation of free radicals and the interaction between terminated polymer chains, monomers and free radicals. Currently, RSGs require extensive work from staff to produce,

use and readout as well as access to expensive machines which have limited free time due to an already large clinical demand.

Characteristically, the gel shows a dose rate dependence and energy dependence within the clinical range. This effect is more pronounced depending on the composition of the gel in use. Additionally, the gels are not tissue equivalent and show some temperature dependence within the clinical range during irradiation.

The primary advantage of gels is their ability to map dose in 3D, the same as is done by film in 2D. This is particularly useful for more complex treatments such as VMAT and IMAT, as well as 3D modelling of dose distribution in low and high dose rate brachytherapy.

2.3 Real-time *in vivo* Dosimeters

2.3.1 Ionisation Chambers

The most extensively used and thoroughly understood of all dosimeters is the ionisation chamber. At its' simplest, an ionisation chamber consists of a region where radiation interacts with a target (the sensitive volume) to produce secondary electrons. This process occurs under bias and produces a current proportional to the initial radiation. The total charge collected is thus proportional to the absorbed dose.

The size, shape, bias voltage and sensitive volume vary depending on the intended use and are often calibrated for use as a reference dosimeter. The primary chamber used in clinical medical physics is the 0.6cm^3 Farmer® thimble ionisation chamber which is pictured in Figure 10. This chamber is particularly useful as there is a wealth of information known about the chamber characteristics and it has reliable response in the clinical energy range [7, 48].

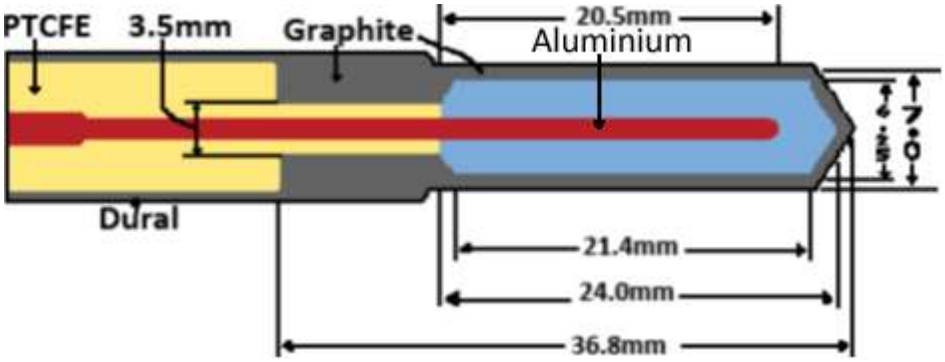

Figure 10: Standard 0.6cc Farmer Ionisation Chamber [22]

2.3.2 Diamond Dosimeters

As discussed previously, there are a number of properties that a detector must exhibit in order to be useful, especially in a clinical setting. Diamond is non-toxic, chemically inert, resistant to radiation damage and most importantly, near tissue equivalent. Synthetic diamond production by chemical vapour deposition (CVD) has significantly reduced the cost of diamond dosimeters. CVD Dosimeters have very high spatial resolution, high sensitivity and good tissue equivalence however some dose rate dependence and temporary loss in sensitivity was observed [49]. Although first investigations into diamond as a sensitive volume began in the 1940's, not enough is understood about the appropriate factors and response for these dosimeters to be widely implemented. With further investigation however there may be an increase in their clinical application.

2.3.3 Metal Oxide Semiconductor Field Effect Transistor Dosimeters

MOSFET dosimeters are solid state transistors which use a change in the electrical characteristics of the junction to determine the incident dose. The potential required to generate a fixed value of current past the junction, the threshold voltage, increases in proportion to the incident dose. Depending on the calibration, sensitivities as high as $5x10^{-4}$ Gy can be obtained from a single chip, with higher sensitivities possible through multiple dosimeter arrangements or variations of the oxide layer [8].

When radiation is incident on a MOSFET dosimeter (shown in Figure 11) electron-hole pairs are produced in the silicon dioxide layer below the gate. Holes may become bound to traps in the silicon dioxide, influencing the flow of charge in the channel between the source and the drain. A positive bias on the gate encourages holes to be trapped closer to the interface between the silicon dioxide layer and the silicon substrate, increasing the effect of the trapped charges on the flow of current in the channel, and hence, increasing the sensitivity. This causes a change in the threshold voltage that is approximately linearly proportional to the initially incident dose [5, 8].

MOSFETs can be produced with extremely small sensitive volumes, giving high spatial resolution, are dose rate independent, can be used for immediate readout, are much easier to use than TLDs and can be used for doses up to 180Gy. However, when using MOSFETs a number of important considerations need to be made. These include: strong temperature dependence, accumulated dose dependence (typically making them unusable after 18500 mV of accumulated dose), lack of tissue equivalence and variation in signal after irradiation [50, 51].

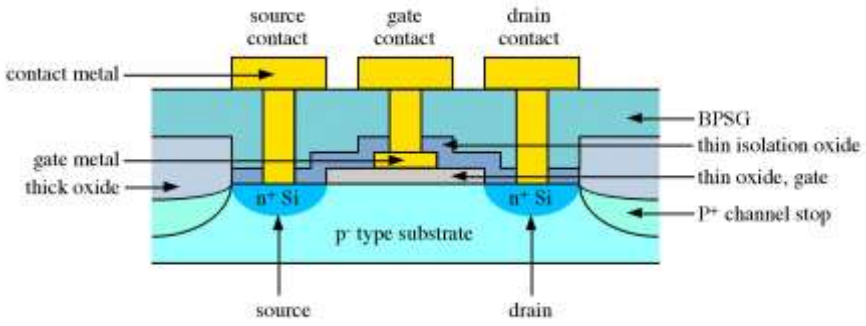

Figure 11: Schematic of MOSFET dosimeter [52]

2.3.4 Dosimetry using Electronic Portal Imaging Devices

Electronic portal imaging devices (EPIDs) are a standard feature on all modern linacs and an integral part of their clinical operation. EPIDs typically consist of arrays of silicon along with a fluorescent material such as CsI and are commonly used to provide images for position verification [53]. Back projection algorithms, (similar to those used for CT image reconstruction) have enabled EPID images to be used to compare both the planned and delivered dose distributions.

Depending on the pixel size, scatter of optical photons in the fluorescent material can cause incorrect binning of counts and in turn affect the 2D dose distribution developed through this method. This limits the spatial resolution of 2D EPID generated dose distributions however, Wendling, Louwe, McDermott, Sonke, van Herk and Mijnheer [54] found that EPID dose distributions were reliable even for more complex treatments such as IMRT. In addition, the availability, convenience and accuracy (within 2% of dose maximum) of EPIDs still make them promising detection method for clinical treatment [54].

2.4 Properties of Clinical Dosimeters

Characterisation of dosimeters is an important process prior to clinical implementation and involves thorough investigation into all relevant dosimeter properties. This includes gathering information about short and long term fading, sensitivity, angular, dose rate and energy dependences, dose linearity, batch homogeneity, tissue equivalence and spatial resolution.

2.4.1 Fading

Fading refers to the inherent loss of signal of a dosimeter over time and has two types, short and long term. Different dosimeters have different fading mechanisms and semiconductor dosimeters fade through spontaneous release of electrons from traps.

In the case of OSL, this can be enhanced through a non-zero ambient light level and as such OSLDs have significant short term fading, shown in Figure 7. The retention of signal after stabilising however was excellent for OSL with dosimeters average reading decreasing by approximately 1.8% from 17 to 38 days after irradiation, becoming stabilised after 27 days [55].

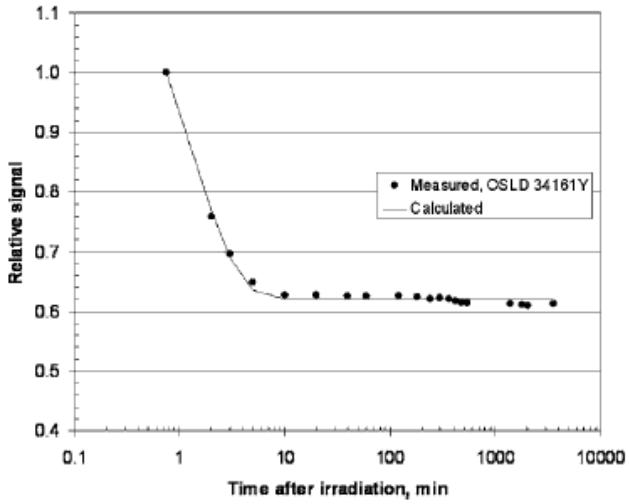

Figure 12: Graph of fading of Al_2O_3:C OSLDs over time [35]

2.4.2 Sensitivity

The relationship between detector signal and incident radiation under the same conditions is not always consistent. Repeated use of the same dosimeter can cause radiation damage to the system, decreasing the signal measured for each subsequent reading.

For OSL, this is caused by destruction of the traps resulting in fewer electrons trapped and less light output on readout. This is shown in Figure 13 from Mrcela, Bokulic, Izewska, Budanec, Frobe and Kusic [56] in which detectors were exposed to 100 and 400cGy 100 times and read after each exposure, a clear loss of response can be seen over the readings.

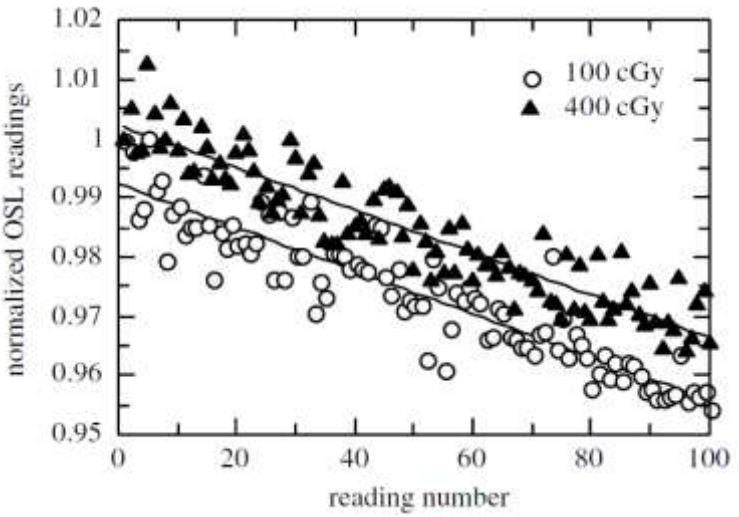

Figure 13: Loss of sensitivity of OSL through multiple readings [56]

2.4.3 Angular Dependence

The response of dosimeters can vary depending on their orientation to the radiation field; this is referred to as angular or directional dependence. Angular dependence is typically due to the detector construction and is a function of the incident energy. As such it is an intrinsic property of the system and needs to be accounted for in detector use [5].

In the case of OSLs, the angular dependence of Al_2O_3:C dosimeters needs to be carefully considered in their clinical implementation. Readings were found to drop by as much as 70% for 25kVp mammography readings and 10-40% for X-ray and CT measurements with the least variation observed for CT [57]. In another study by Kerns, Kry, Sahoo, Followill and Ibbott [58], a 4% and 3% decrease in reading was observed for 6 and 18 MV beams respectively, this supported results found by using Al_2O_3:C dosimeters and 6 MV radiation fields [35]. This suggests that for clinical dosimetry, Al_2O_3:C dosimeters are best used for higher energy fields and placed as perpendicular to the field as possible.

2.4.4 Energy Dependence

Energy dependence is a term regularly used throughout the literature but often poorly clarified. It is generally a ratio of detector response to a standardised response, such as response per unit absorbed dose in water or exposure in air from Co-60 reference radiation. In the context of OSL this refers to the number of electrons liberated for a given radiation energy in comparison to the reference [9]. Each definition of energy dependence is based on a number of fundamental assumptions regarding the nature of the interactions within the dosimeter and the existence of charged particle equilibrium (CPE).

More broadly, energy dependence can be quantified as the ratio of the dosimeter reading to the dosimetric quantity, that is the reading displayed compared to the ideal reading[5]. An example of this is shown in Equation 16. The ratio is taken in comparison to response per unit absorbed dose in water. [5]

$$\frac{(\frac{r}{D_{water}})_{\bar{E}}}{(\frac{r}{D_{water}})_{1.25}} \cong \frac{\vartheta_{\bar{E}}}{\vartheta_{1.25}} \; where \; \vartheta = \frac{(\frac{\mu_{en}}{\rho})_g}{(\frac{\mu_{en}}{\rho})_{water}} \tag{19}$$

Equation 19: Homogeneous dosimeter energy dependence

2.4.5 Tissue Equivalence

Tissue equivalence refers to the radiation equivalence of the detector materials to water, a common approximation for a variety of soft tissues in the body. Tissue equivalence depends on the effective atomic number of the dosimeter, the quality of the radiation and a tissue equivalent detector can remove the need for correction factors and significantly reduce calculations for a detector system [59, 60].

3. EXPERIMENTAL INVESTIGATION

3.1 Introduction and Materials

In order for a detector to be considered thoroughly characterised a wide array of properties need to be understood. For this study, several detector properties were examined separately through an individual experiment designed to isolate that particular property. The basic setup of each experiment involved an arrangement of solid water, one or more OSLDs and the Varian IX linear accelerator in operation at the Shoalhaven Cancer Care Centre. Readout was performed using a Landauer InLight microStar system (pictured in Figure 14) with the system operating in NanoDot® mode, after running initial tests, the manufacturer determined calibration factor of 1000 and crossover value (point at which weak stimulation is used to protect the PMT) were used.

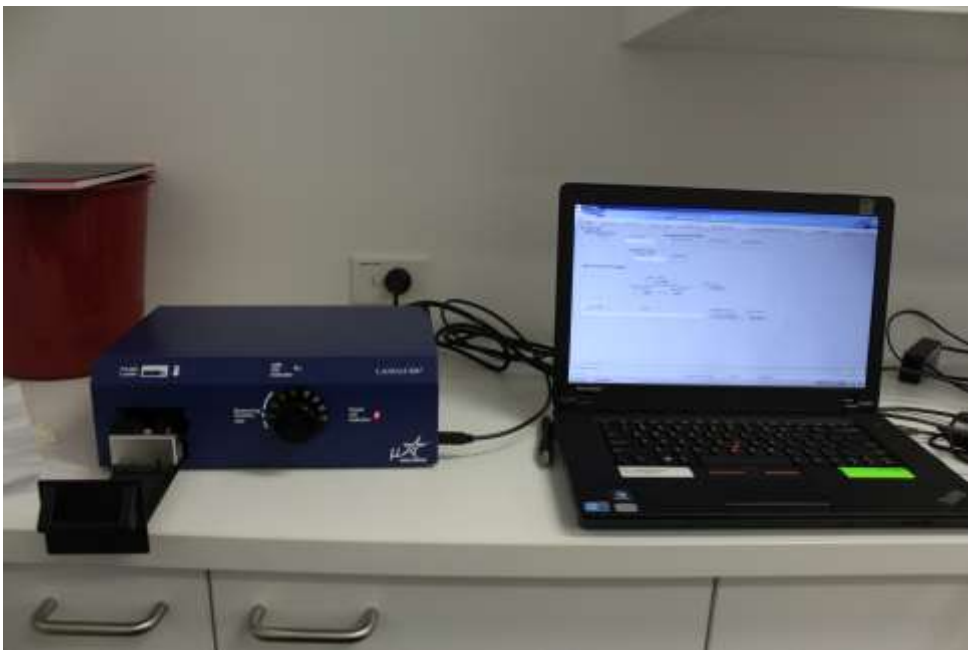

Figure 14: Landauer InLight microStar OSL readout system

For many of the experiments, a control was needed with which the OSLD signal could be compared. To this end a, water tight, graphite tipped, 0.6cm^3 Farmer ionisation chamber was

used. This chamber was used in the commissioning of the linear accelerator and also provided an effective method of ensuring the machine was operating correctly.

Due to the different density of air and the effect of air on radiation transmission, a 1cm sheet of Superflab® was placed over the detector. The Superflab provided a tight contact with the detector to remove air gaps and also provided a smooth surface for the solid water placed above the detector. Although the density and composition of this material is not identical to the solid water or tissue, it is as close possible and is a commonly used clinical bolus material [61]. The remainder of the build-up region was then constructed from solid water to place the detectors at d_{max} for all measurements, unless specified otherwise.

3.2 Preliminary Investigation - Annealing Tests

OSLDs which have been irradiated have electrons trapped within their structure that provide the signal when readout occurs, however a detector which has residual signal on it would not be useful for future measurements. Like other solid state dosimeters, OLSDs can be "annealed" to allow them to be reused repeatedly until physical or radiation damage occurs. This process for OSLDs however is still being perfected for clinical application and current literature lists a variety of methods, from irradiation by 6 x FL-15 UV lamps [62] to 1 minute exposure with an endoscopic illuminator [35]. For this study, a Gammasonics® manual OSL annealing lightbox consisting of a one sided arrangement of fluorescent lamps was used to anneal (see Figure 15).

Figure 15: Gammasonics® OSL manual annealing lighbox

3.2.1 Aim

The aim of this investigation was to determine the optimal time required for thorough annealing of the OSLDs due to limited literature being present on correct use of the supplied manual annealing lightbox.

3.2.2 Materials and Method

Eight detectors were irradiated by 6 MV at 600MU/min and d_{max} then read out before being annealed for between 2 minutes and 2 hours to determine an optimal annealing time. The annealing process consisted of manually sliding the Al_2O_3:C sensitive volume out of the plastic casing and placing the open detector onto the surface of the lightbox shown in Figure 15. The duration of the annealing process was determined by a timer on the front of the lightbox and after the lightbox was activated the detectors were exposed to low intensity fluorescent light for a prolonged period of time. Based on the Gammasonics® manual advising "UV Light from sources such as unshielded fluorescent lamps or sunlight can result in an increase in residual dose." [63] only optical light is used in the annealing process; however light source information is deemed to be proprietary by the distributor.

3.2.2.1. Error Calculation

To ensure data throughout this thesis is correctly represented, where possible associated errors are included. Errors were determined based on a normal distribution of data, to ensure a normal distribution the data range was compared to 3 times the standard deviation of the set.

$$\sigma = \sqrt{\frac{< x^2 > - < x >^2}{n}} \tag{20}$$

Equation 20: Relation between Standard Deviation (σ), average (< >) of values (x) and total number of values (n) [5]

Given a normal distribution of data (such as is the case here), errors can be expressed using multiples of the standard deviation, called a confidence interval. Twice the standard deviation is used to give a 95% confidence interval. The 1.96 figure is obtained from an approximation of the Normal cumulative distribution function [64].

$$95\%\ Confidence\ Interval = 1.96 * \sigma \quad (21)$$

Equation 21: Derivation of 95% confidence interval used in error expression [5]

3.2.3 Results

At low annealing times, minimal dose was removed and as such some detectors were annealed repeatedly with dose variations recorded

Table 1 shows the results of a variety of annealing times, these dosimeters were irradiated through the course of becoming accustomed to the equipment and experimental conditions for these exposures varied. The detectors used for previous experiments were annealed for 12hrs in an attempt to remove residual dose and this is shown in Table 2.

Table 1: Initial OSL annealing results

Dosimeter Number	Time Annealed (s)	Initial Dose (cGy)	Final Dose (cGy)	Percent Annealed (%)
64904K	120	206.53 ± 4.75	130.46 ± 3.00	36.83
64904K	536	130.46 ± 3.00	20.61 ± 0.47	84.20
86738A	120	205.54 ± 4.73	147.06 ± 3.38	28.45
86738A	1176	120.65 ± 2.77	6.33 ± 0.15	94.75
64523U	1800	194.86 ± 4.48	7.89 ± 0.18	95.95
04733W	3000	188.06 ± 4.33	3.81 ± 0.09	97.97
37973M	5400	200.77 ± 4.62	1.29 ± 0.03	99.36
57007W	7200	194.23 ± 4.47	0.518 ± 0.01	99.73

Table 2: 12hr anneal of used dosimeters

Dosimeter Number	Initial Dose (cGy)	Final Dose (cGy)	Percent Annealed (%)
333602	205.78 ± 4.73	1.76 ± 0.04	99.14
60947D	204.77 ± 4.71	7.93 ± 0.18	96.13
36347O	199.93 ± 4.60	1.61 ± 0.04	99.19
64345S	199.01 ± 4.58	1.17 ± 0.03	99.41
60892K	197.4 ± 4.54	1.71 ± 0.04	99.13
86890I	197.3 ± 4.54	1.48 ± 0.03	99.25
60877C	196.59 ± 4.52	1.18 ± 0.03	99.40
64885C	195.11 ± 4.49	1.59 ± 0.04	99.19
64754J	194.97 ± 4.48	1.24 ± 0.03	99.36
64726K	191.44 ± 4.40	0.84 ± 0.02	99.56
94519J	190.77 ± 4.39	1.75 ± 0.04	99.08
64584M	189.61 ± 4.36	1.23 ± 0.03	99.35
64745I	185.85 ± 4.27	0.94 ± 0.02	99.49
57193T	93.03 ± 2.14	0.81 ± 0.02	99.13
86891G	47.43 ± 1.09	0.25 ± 0.01	99.47
64904K	17.22 ± 0.40	0.97 ± 0.02	94.37
60860R	8.35 ± 0.19	0.64 ± 0.01	92.34
64523U	7.64 ± 0.18	1.12 ± 0.03	85.34
86738A	6.22 ± 0.14	0.83 ± 0.02	86.66
04733W	3.75 ± 0.09	0.9 ± 0.02	76.00
56838C	3.51 ± 0.08	0.14 ± 0.01	96.01
37973M	1.24 ± 0.03	0.46 ± 0.01	62.90
64722Q	1.012 ± 0.02	0.099 ± 0.01	90.22
57007W	0.51 ± 0.01	0.34 ± 0.01	33.33

Based on the average of 5 unirradiated dosimeters background reading being 0.054±0.0027cGy, an annealed dosimeter was defined as one with no reading greater than 0.1cGy. This limit was chosen to improve precision, particularly for low dose measurements. As such, based on the results shown in Table 2, a third experiment was designed in which a set of 5 dosimeters were irradiated by 6 MV at 600MU/min when positioned at 1.5cm depth for 200MU (expected to give a dose of 200cGy). These detectors were then annealed for 24hrs and the results (in Table 3) showed all dosimeters were below the 0.1cGy limit indicating that this would be appropriate for further experiments.

Table 3: Initial and Final dose of 24hr anneal

Dosimeter Number	**Initial Dose (cGy)**	**Final Dose (cGy)**
64724O	201.32 ± 4.63	0.028 ± 0.001
875698	203.17 ± 4.67	0.041 ± 0.001
64549G	200.11 ± 4.60	0.042 ± 0.001
64543S	207.43 ± 4.77	0.036 ± 0.001
57183U	204.61 ± 4.71	0.039 ± 0.001

Although initial experiments indicated that 24hr would be sufficient time to thoroughly anneal the dosimeters using the manual annealing lightbox, the average initial (background) dose prior to each experiment was monitored. This showed a notable and consistent increase in the average background dose over several weeks and experiments.

As a result of this trend, a 36hr annealing experiment was performed to test if it was possible to ensure the background would always stay below the 0.1cGy limit set. The average background dose for the first 20 experiments conducted is shown in Figure 16, the 4th experiment was the final one performed following a 24hr anneal, all subsequent

experiments were performed after a 36hr anneal. Additionally, all experiments listed in the following chapters reference only those where a 36hr anneal was used as this was found to be more effective to keep background dose below the limit.

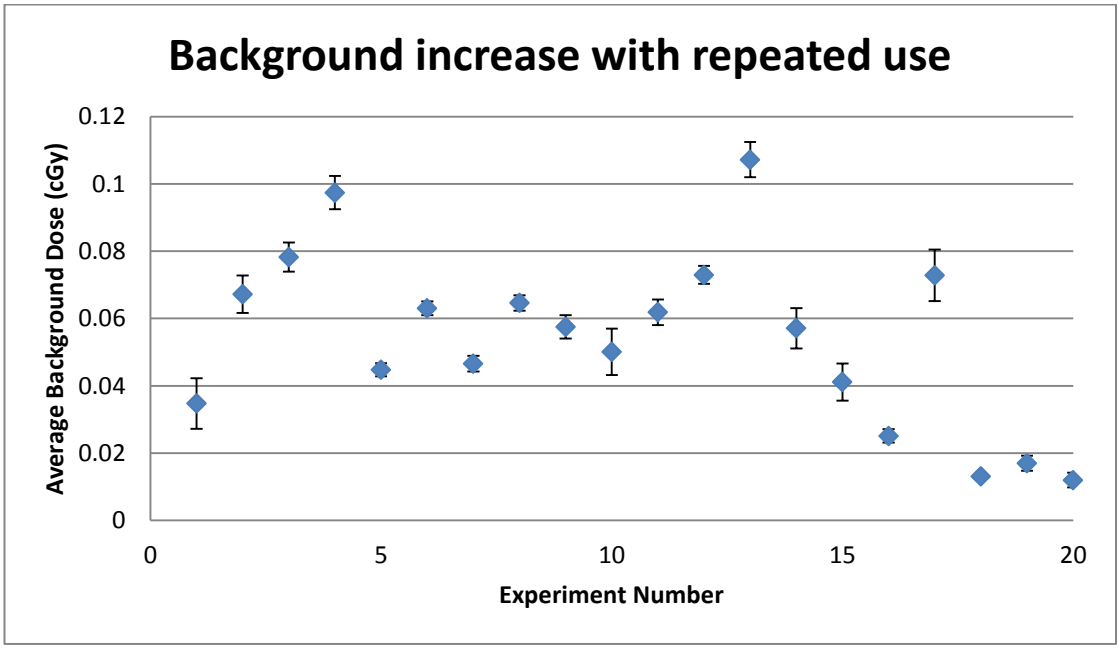

Figure 16: Background dose trend after repeated use (95% confidence interval)

3.2.4 Discussion

Through methodical escalation of annealing time, a 36hr anneal time was selected which, whilst long and possibly not clinically ideal, ensured that the anneal was reliably thorough and complete. The 0.1cGy limit was chosen based on a combination of the level of precision required for low dose clinical investigations and the typical background of dosimeters that had not previously been irradiated. Other more intense sources of illumination could be used if the 36hr time becomes prohibitive however this is not foreseen to be an issue.

3.3 Preliminary Investigation - Batch Sensitivity

Despite being manufactured from the same material and even from the same batch of the same material there will always be notable variation in the sensitivity between two

otherwise identical detectors. Radiation induced damage or variations in dopant concentration in the crystalline structure can make one dosimeter slightly more or less sensitive than another [65].

In an attempt to account for this, the Landauer NanoDots® are shipped with pre-assigned sensitivities. The derivation and meaning of these sensitivities however are not discussed in the supplied literature and the radiation source used is a Co-60 source which produces 1.17 and 1.33MeV gamma rays. In order to correct for any energy dependent sensitivity variation between the discrete peaks of the Co-60 source and the higher energy spectrum delivered by a clinical linear accelerator, the manufacturer sensitivities were ignored and new batch sensitivity values were recalculated. Quoted results throughout the remainder of this work have had the manufacturer values factorised out.

3.3.1 Aim

To determine batch sensitivity values for 48 OSLs at 6 and 10 MV to account for energy dependence compared with manufacturer sensitivities as determined with a Co-60 source.

3.3.2 Materials and Method

The entire batch of 48 dosimeters were arranged in a 7 x 7 grid, excluding location 49, as shown in Figure 17 and placed at a depth of 10cm in solid water with 10cm of backscatter. The field size and number of monitor units were kept consistent throughout at 20cm x 20cm and 200MU respectively. Dosimeters were placed at 10cm depth to ensure a flat field across the grid which was independently verified prior to performing experiments using data gathered during normal clinical operation. For each round of experiments, every detector was read 3 times immediately before and 1hr after irradiation. Following readout, the batch was annealed for 36hrs and 3 full read-irradiate-read cycles were completed at both 6 and 10 MV energies.

3.3.3 Results

After significant investigation, the average sensitivity values are shown in Figure 18 and Figure 19 for 6 and 10 MV respectively. The relationship between dosimeter grid position and dosimeter ID number is also summarised in Table 4 and Figure 17.

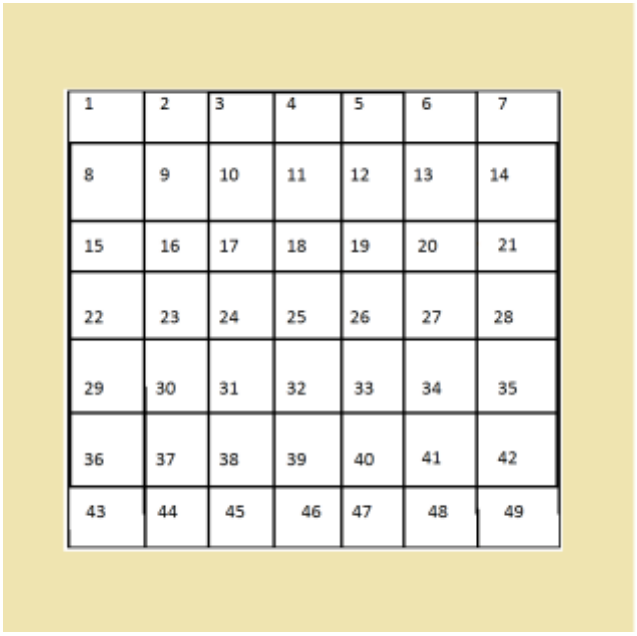

Figure 17: Arrangement of OSLs in grid positioned in beam field (shown in yellow)

Table 4: Relation between dosimeter and grid position during sensitivity measurement

Dosimeter Number	Grid Position	Dosimeter Number	Grid Position	Dosimeter Number	Grid Position
60896C	1	64739B	18	60947D	35
04747N	2	64894D	19	37973M	36
333602	3	82641O	20	86738A	37
64519J	4	60897A	21	64904K	38
60877C	5	36346Q	22	64754J	39
60860R	6	86891G	23	36347O	40

64584M	7	56838C	24	647888	41
64745I	8	57007W	25	04733W	42
64345S	9	86906D	26	60892K	43
56839A	10	569976	27	875698	44
82663I	11	64523U	28	64545S	45
56990K	12	86890I	29	57183U	46
64885C	13	64726K	30	64549G	47
64728E	14	60847F	31	64724O	48
64324W	15	643402	32		
57193T	16	64722Q	33		
56992G	17	64579D	34		

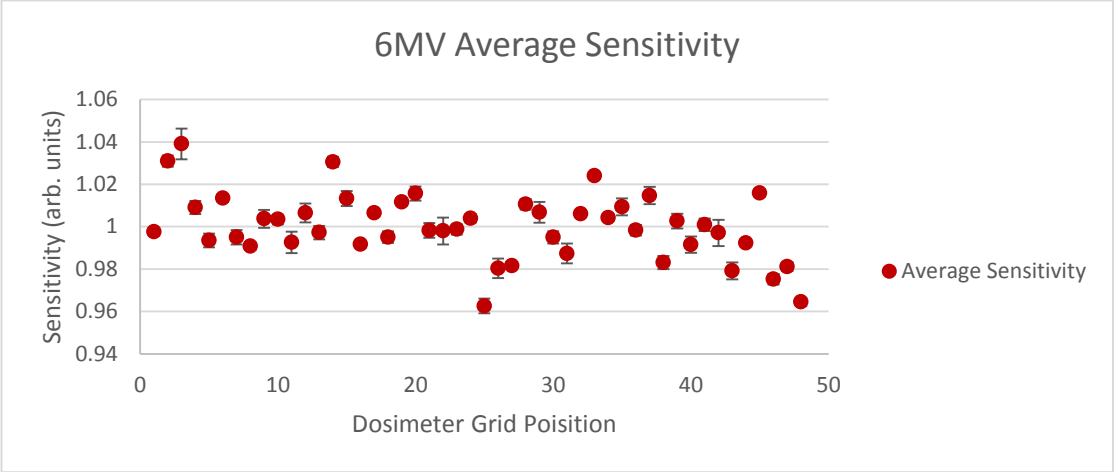

Figure 18: 6 MV Batch Sensitivity Averages

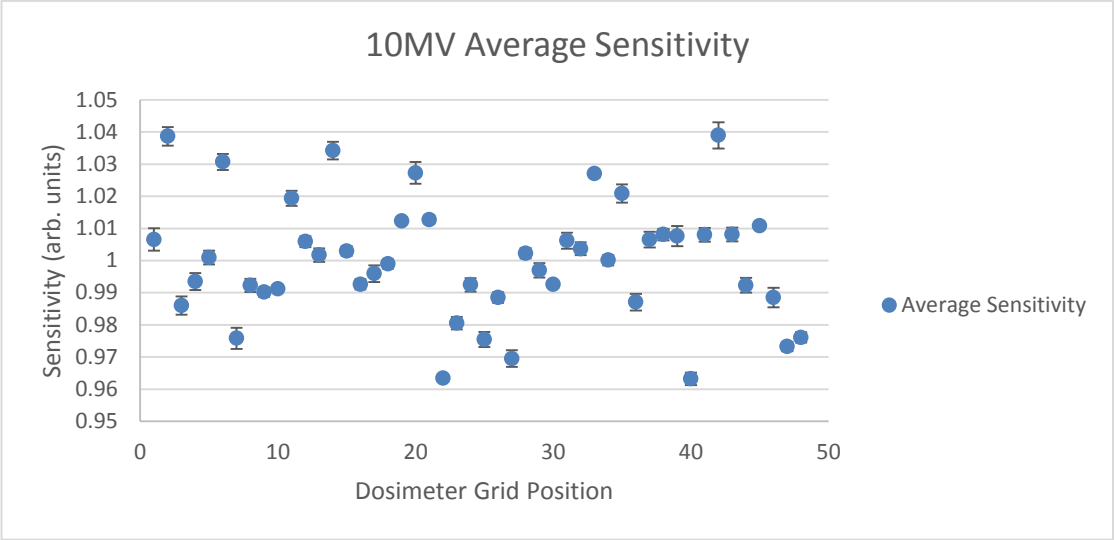

Figure 19: 10 MV Batch Sensitivity Averages (95% conf. int. shown)

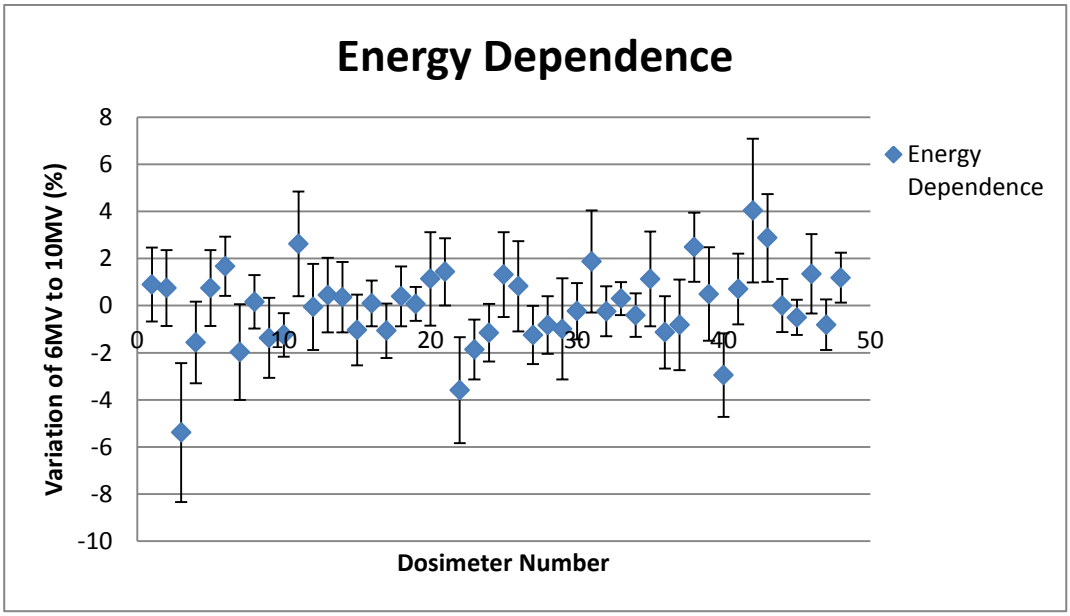

Figure 20: Variation in sensitivity at 6 & 10MV for each dosimeter (%) (95% conf. int. shown)

3.3.4 Discussion

Figure 18 and Figure 19 outline the relative batch sensitivities for 6 and 10 MV respectively with 95% confidence interval. It was found that there was minimal variation across the batch, with the highest sensitivity being 1.038 and lowest being 0.963, suggesting that despite the large number of factors that may affect OSL response, the NanoDot® has reasonably uniform structure from one dosimeter to another.

These results were then used to examine the energy dependence. The sensitivity values obtained for each dosimeter at 6 and 10MV were divided and the deviation of this ratio from unity for each dosimeter is shown in Figure 20. The average of all 48 dosimeters was 1.0002 ± 0.0007 (or 0.02% difference in the sensitivity at 6 and 10MV) which indicates that NanoDot® OSLDs exhibit minimal energy dependence at therapeutic energies. This finding is supported by the work of Yukihara and McKeever [55], Akselrod [66], Viamonte, da Rosa, Buckley, Cherpak and Cygler [67], who found that at therapeutic energies NanoDot® energy dependence is limited.

4. DOSIMETER PROPERTIES

4.1 Short Term Fading

4.1.1 Introduction

The role of NanoDot® OSLs in clinical practice primarily revolves around them being used for quick checks of sensitive volumes and margins. Due to the simple and quick readout procedure as well as their inherent robustness, they function as an excellent *in vivo* dosimeter. An intrinsic part of this is the ability to be read out rapidly without delaying further treatment as well as providing information about the effectiveness of a currently implemented treatment plan which may result in changes to the plan or its delivery method.

Like any dosimeter, OSLs exhibit both short and long term fading. In the case of OSLDs this is due to spontaneous emission. Short term fading of materials that exhibit OSL is a very complex field. The appropriate mathematical description of emission probability is dependent on the material, temperature of readout, laser operation (continuous, linearly increasing or pulsed) and wavelength of laser used. Due to the variability and complexity of emission formula, readers are directed to Botter-Jensen, McKeever and Wintle [68].

In the case of the implementation of NanoDot® OSLs, long term fading is not clinically relevant and as such only short term fading was dealt with in this study. Since most clinical treatments involve regular visits and dosimeters will be read out within 48 hours, this was chosen as the time interval over which the fading was monitored.

4.1.2 Aim

To determine the short term fading characteristics of NanoDot® OSLs over a 48hr period. This will be achieved through readouts spaced across 48hrs with a higher number of readings in the initial 4hrs to accurately plot the steep signal decrease expected.

4.1.3 Materials and Method

Since the time interval was substantial, the number of dosimeters used was determined by how many data points were required to adequately represent the fading curve. From previous literature[30, 35] it was determined that the region of most variation was the initial two hours. To adequately cover this region of rapid change, detectors were read out at 1,2,5,10,15,30,60,120,240,360,480 minutes following irradiation, then over the subsequent two days at longer intervals.

Prior to irradiation, all dosimeters were annealed for 36 hours and then read out three times to determine an average background dose. The experimental setup was as per Figure 21 and following irradiation each detector was left for one of the set time intervals and then read out three times in quick succession (taking roughly 30-45seconds).

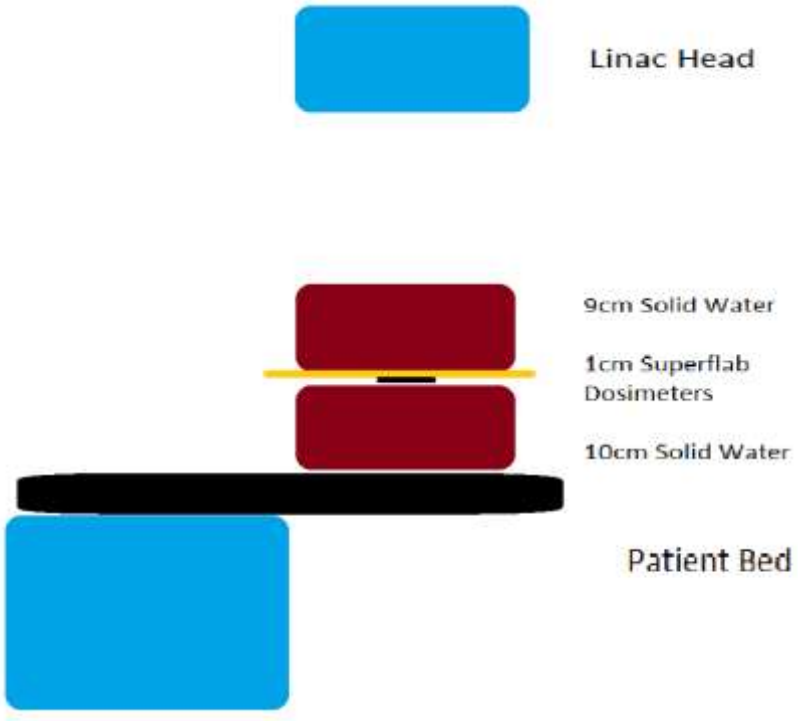

Figure 21: Experimental setup for 6 MV Short term fading

The detectors were arranged in a grid in the centre of a 20cm x 20cm field and irradiated by 6 MV to 200MU at 10cm depth. 6 MV was used as this is the energy most commonly used clinically and similar results are expected at 10 MV.

4.1.4 Results

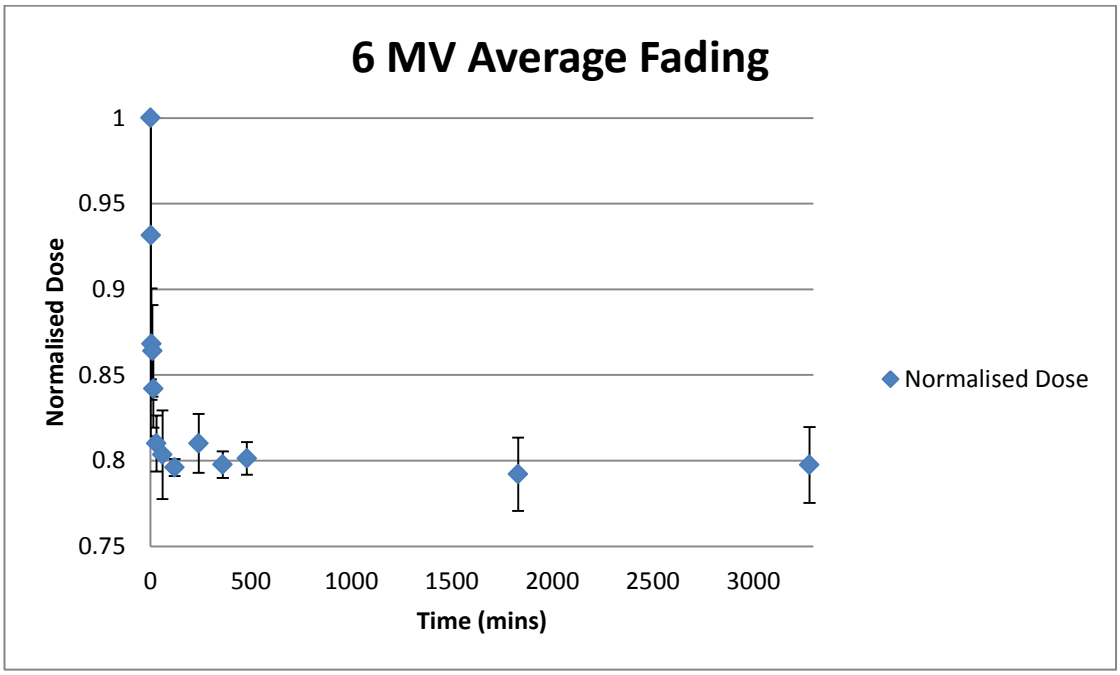

Figure 22: 6 MV Short Term Fading results with 95% confidence interval

As shown in Figure 22, there is a significant drop in relative signal strength in the immediate time following irradiation however after this period the signal remains relatively stable for the remaining 48 hours. It was determined that it takes 30-60 minutes for the OSLD signal to stabilise which suggests this should be the waiting time between irradiation and readout for maximum accuracy and reliability.

4.1.5 Discussion

The significant (almost 20%) fading during the initial period following irradiation is expected from a solid state dosimeter as unstable traps lose electrons. This result however is considerably different from that obtained by Jursinic [35] in which there was a 35% fading

trend observed in the first 8 minutes following irradiation but may be attributed to hardening of the beam due to differences in experimental setup, giving an effectively higher energy beam.

From the results obtained with this experimental set up and dosimeter batch, all future measurements were performed with a 45-60 minute wait time following irradiation to ensure adequate time was allowed for the signal to stabilise. Additionally, based on this data, dosimeters can be reliably read up to 48 hours following irradiation.

4.2 Signal Loss Per Readout

4.2.1 Introduction

The mechanism behind OSL in Al_2O_3:C provides a stable system of signal retention if the dosimeter is not read. Through better PMT technology, this proportion of signal loss can be reduced, however the amount of signal loss from a reading and the number of reliable readings from a single dosimeter both need to be determined.

The readout procedure of dosimeters is one important criterion to their use with passive and real time dosimeters having distinct advantages. In addition to this, some dosimeters can only be irradiated once such as film, whilst others measure accumulated dose before having the signal annealed and being re used.

4.2.2 Aim

To determine the proportion of signal loss as a result repetitive irradiation, readout and annealing.

4.2.3 Materials and Method

Similar to previous experiments, 5 dosimeters were irradiated by 200MU at 6 MV when positioned under 1cm of Superflab® and 0.5cm of solid water with 10cm back scatter. This experiment was conducted at d_{max} as the dose delivered was not being examined; only the relative signal drop during readout. Each dosimeter was readout three times before the experiment and then read 100 times in succession (to limit effect of short term fading). The background established before irradiation was then subtracted and previously determined 6 MV batch sensitivity factors were applied to give signal drop due to readout.

4.2.4 Results

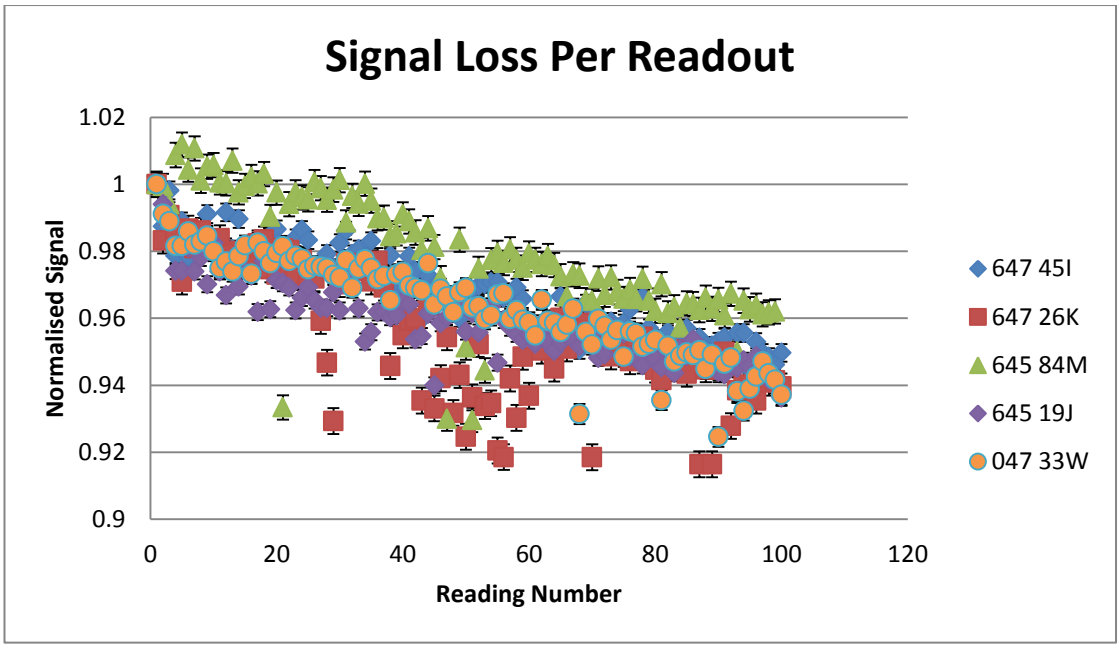

Figure 23: Signal loss per readout for 5 dosimeters

Figure 23 shows the effect of readout on signal loss, the procedure used for signal readout of OSLs allows for multiple readouts and is a major feature of solid state detectors. However, if a significant number of readouts are made the loss from readout needs to be accounted for.

4.2.5 Discussion

Through a line of best fit the rate of signal loss can be described mathematically. Although apparently linear the rate of signal loss is actually a proportion of signal retained in the traps. Whilst a linear fit would describe this data set and appear more pictorial, this is conditional on the number of readings remaining small. The exponential description is used here as it is more robust and better describes the underlying physical principle. Equation 22-24 shows the decay function for each dosimeter, where x is the repeat readout number. Equation 20 shows the decay function of the average of all 5 dosimeters:

$$y = 1.0041e^{-0.0005x} \quad (22)$$

Equation 22: Decay function of dosimeter 645 84M

$$y = 0.9901e^{-0.0004x} \quad (23)$$

Equation 23: Decay function of dosimeter 647 45I

$$y = 0.9814e^{-0.0004x} \quad (24)$$

Equation 24: Decay function of dosimeter 647 26K

$$y = 0.9777e^{-0.0004x} \quad (25)$$

Equation 25: Decay function of dosimeter 645 19J

$$y = 0.9886e^{-0.0005x} \quad (26)$$

Equation 26: Decay function of dosimeter 047 33W

$$y = 0.9883e^{-0.0005x} \quad (27)$$

Equation 27: Average Rate of signal loss per readout

This suggests that the signal loss per readout is 0.0005 (or approximately .05%) of the current signal. Whilst this is small, with multiple readouts it is necessary to correct for as the contribution to error can become significant. The observable drop in signal of 4% at approximately 40 readouts is noticeable for at least 3 of the 5 dosimeters. Beyond 40 readings the dosimeter readout is observed to become unstable and remain unstable for subsequent readouts, this is particularly noticeable for 64726K (shown in red). Further investigation would be required to determine the cause of this effect, however the 40 readouts required for this effect to present is significantly more than the 1 or 2 used clinically. As a result of this, it is advisable to limit clinical readouts to no more than 15-20, which is expected to be more than sufficient.

4.3 Reproducibility

4.3.1 Introduction

Multiple factors can affect the accuracy and precision of a reading, as such, determining the magnitude and cause of these factors is important to correct for those that are deemed significant.

One such factor is the variation in a dosimeters' response day-to-day. This can be caused by variation in the environmental conditions between days such as humidity and temperature, as well as variation in the radiation source. The sensitivity of OSLs to these variations needs to be determined before they are used clinically, although hospital conditions are maintained within the guideline provided by Workcover NSW [69] of 16-20^{o}C and humidity of 40-70%, this may still be enough to cause variation in dosimeter response.

4.3.2 Aim

To examine the variation of OSL dosimeters over multiple days to determine day-by-day variation.

4.3.3 Materials and Method

As with previous experiments dosimeters will be irradiated with 100MU at 6 MV in a 10cm x 10cm field. The 3 dosimeters used were irradiated separately and positioned in the centre of the field each time. The dosimeters were positioned at a depth of 6cm (5cm of solid water and 1cm of SuperFlab®), to provide a reference between measurements a 0.6cc Farmer Ionisation chamber was positioned at a further 5cm depth with 10cm of backscatter beneath. The ionisation chamber used was kept consistent throughout the experiment and a -300V bias was used. The experimental setup is pictured in Figure 24 for reference, note that

the depth was due to available solid water and does not affect results as only the relative signal is important.

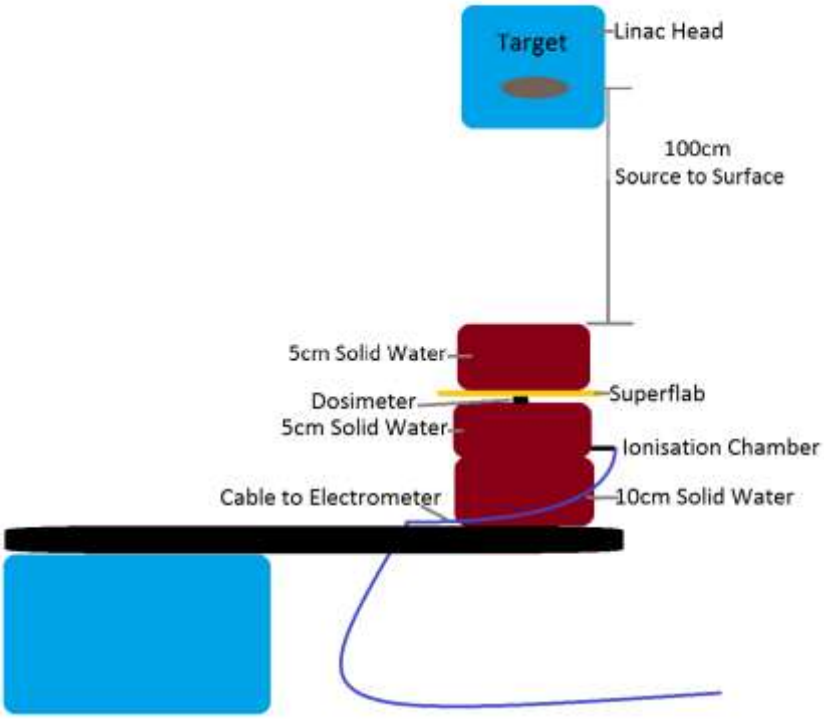

Figure 24: Reproducibility Setup

The current from the ionisation chamber during irradiation was used to correct for temperature and pressure variations between measurements, both were determined prior to irradiation using an electronic temperature probe and electronic barometer. This information was then used according to TRS-398 to correct the signal; the equation for determining the factor, k, used to correct ionisation chamber measurements is shown in Equation 28: [48]

$$k_{TP} = \frac{(273.2 + T)P_0}{(273.2 + T_0)P} \tag{28}$$

Equation 28: Correction factor, k, for ionisation chambers

Each dosimeter was read three times prior and post irradiation with the dose quoted as the difference between these two values. The values were then corrected by removal of the supplier sensitivities, then the batch sensitivities previously determined were applied.

4.3.4 Results

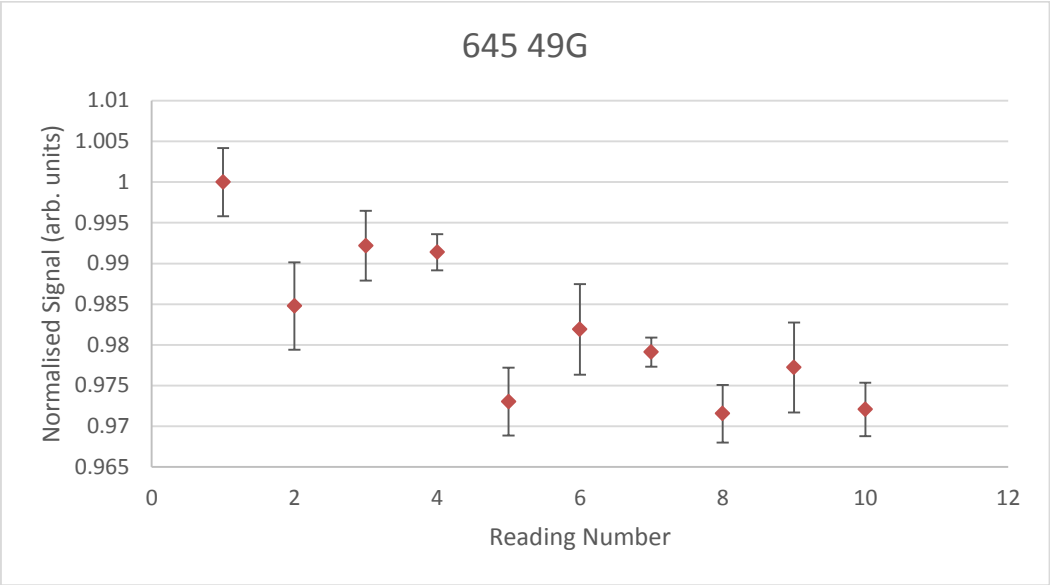

Figure 25: Dosimeter 64549G variation over 10 readouts

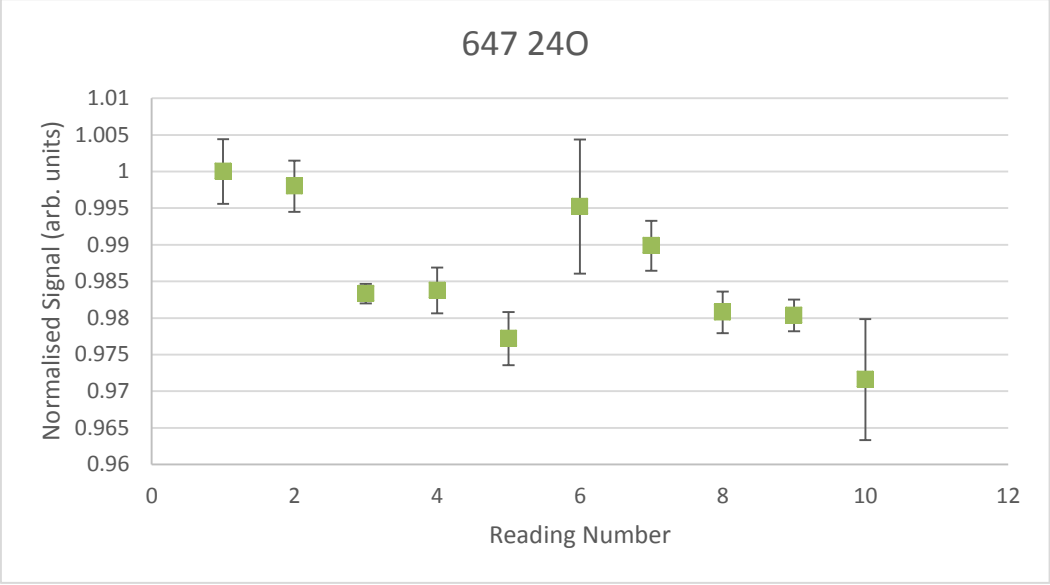

Figure 26: Dosimeter 64724O variation over 10 readouts

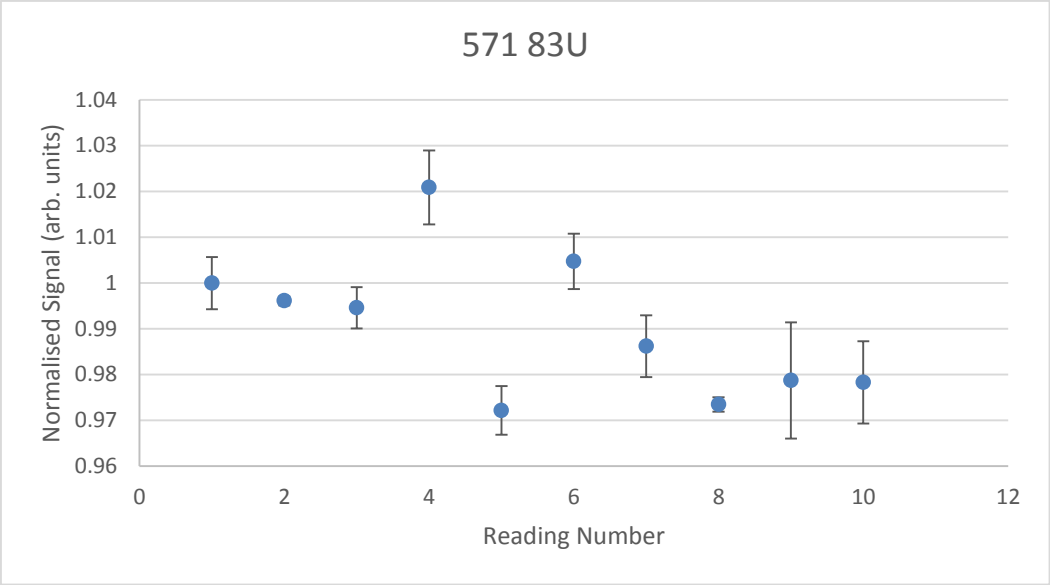

Figure 27: Dosimeter 57183U variation over 10 readouts

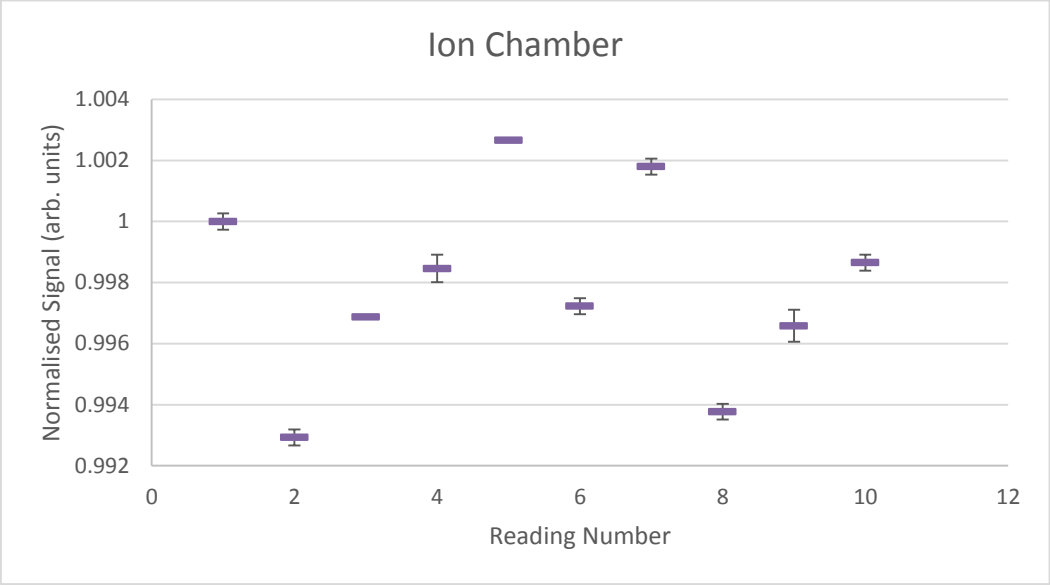

Figure 28: 0.6cc Farmer Ionisation chamber variation over 10 readouts

The use of the Ionisation chamber as a reference is justified by Figure 28, where the error in the readings is at most ±0.05% with a portion of that most likely due to environmental or equipment variation. For the OSLDs however, at a 95% confidence interval the largest normalised errors were ±0.57, 0.92 and 1.29% respectively.

4.3.5 Discussion

Across the 10 readings, the variation in the Ionisation chamber is negligibly small and could be put down to other factors such as cable noise. The OSLDs however had variation across the range of 2.84, 2.84 and 4.87% respectively, giving an average variation of 3.52 ± 0.998%. In most clinical cases, this will be of statistical significance and justifies the averaging of multiple readouts and/or multiple detectors to minimise this impact. Given the limited useful lifetime of the OSLDs, the use of 3 measurements per data was deemed sufficient when using expendable materials and given the 95% confidence interval error was at most 1.29%.

4.4 Dose Linearity

4.4.1 Introduction

Although all dosimeters record signal at all doses, due to a variety of intrinsic properties, detectors will only precisely record dose within a fixed range. The size and location of this range depends on the type of dosimeter and greatly varies. In the case of OSLDs for clinical use, a linear range of 0-200cGy would be the minimum required with a linear range up to 500cGy, ideal to enable use of OSLDs on hypofractionated prostate and breast patients [70].

4.4.2 Aim

To determine the linear range of response of OSLDs for clinical application through gradual dose escalation.

4.4.3 Materials and Method

Setup is identical to that shown in 4.3.3, however the dosimeter was positioned below 4cm of solid water and 1cm of SuperFlab®, and 10cm of backscatter material was positioned below. Prior to each set of measurements, the SuperFlab® was swapped with a 0.6cc Farmer ionisation chamber and a set of 3 chamber measurements were taken for reference.

For each set of monitor units, 3 dosimeters were irradiated and each was read out 3 times prior and post irradiation. The average of these 9 readings was taken to represent each point and compared against the average of the 3 ionisation chamber measurements.

4.4.4 Results

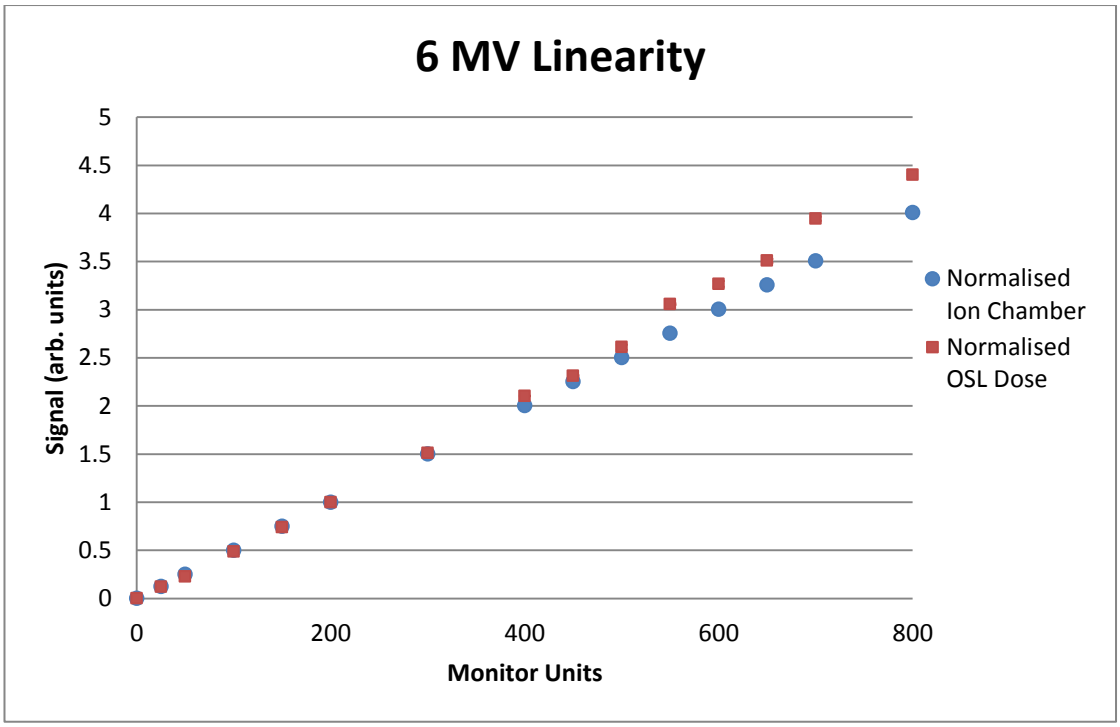

Figure 29: OSLD and 0.6cc Farmer Ionisation chamber linearity up to 800MU (Maximum error 0.026%)

Figure 29 plots the number of monitor units against the signal. Whilst the ionisation chamber has near perfect linearity across the entire range examined, the OSLD values vary. The data has been normalised to 100MU for easiest comparison and it can be seen that allowing for the impact of other factors discussed throughout this work, the data is approximately linear.

4.4.5 Discussion

Although the OSLDs do not display the same linearity as an ionisation chamber, in the range of interest for clinical investigations (0-500MU) they responded in a near linear fashion. The deviation from linearity is significant beyond 500MU. These results also agree with previous results obtained by: Jursinic [35], Hu, Wang and Zealey [71] & Viamonte, da Rosa, Buckley, Cherpak and Cygler [67]. The response of most clinical significance is in the range of 0-200MU, which is also the region of best linearity, suggesting OSLDs would be appropriate across the common clinical range.

4.5 Dose Rate Dependence

4.5.1 Introduction

The mechanism of signal generation has been discussed extensively as it is the source of many of the characteristics unique to OSLs. In the case of dose rate dependence this is no different; the lifetime of the phosphorescence centres varies with the depth of the trap but will always be a finite value. In the case of Al_2O_3:C this is 35ms and signal stability will only occur once the rate of signal trapping balances the rate of thermal release [65].

The rate of stimulation and excitation in OSLs can be described by similar simultaneous equations to those used for TLDs. Using numerical simulation and setting initial conditions to typical values, Chen and Leung [72] predicted dose rate dependence for OSLs. This is contrary to the numerical and empirical data gathered by Pingqiang, Zhaoyang, Yanwei, Turun and Yun [29] using CaS:Ce,Sm, however using the same system as is being examined here, Viamonte, da Rosa, Buckley, Cherpak and Cygler [67] obtained an increasing response with increasing dose rate. This wide range of results suggests that OSL dose rate dependence varies on conditions such as the type of OSL material being used.

4.5.2 Aim

To determine whether Al_2O_3:C OSLDs exhibit dose rate dependence under typical clinical conditions, by exposure to multiple dose rates.

4.5.3 Materials and Method

The experimental setup was identical to that used for the Reproducibility investigation (see 4.3.3 and Figure 24 for details and diagram). For consistency with other experiments 6 MV was used and 100MU was delivered at a variety of dose rates with 100cm SSD maintained throughout.

4.5.4 Results

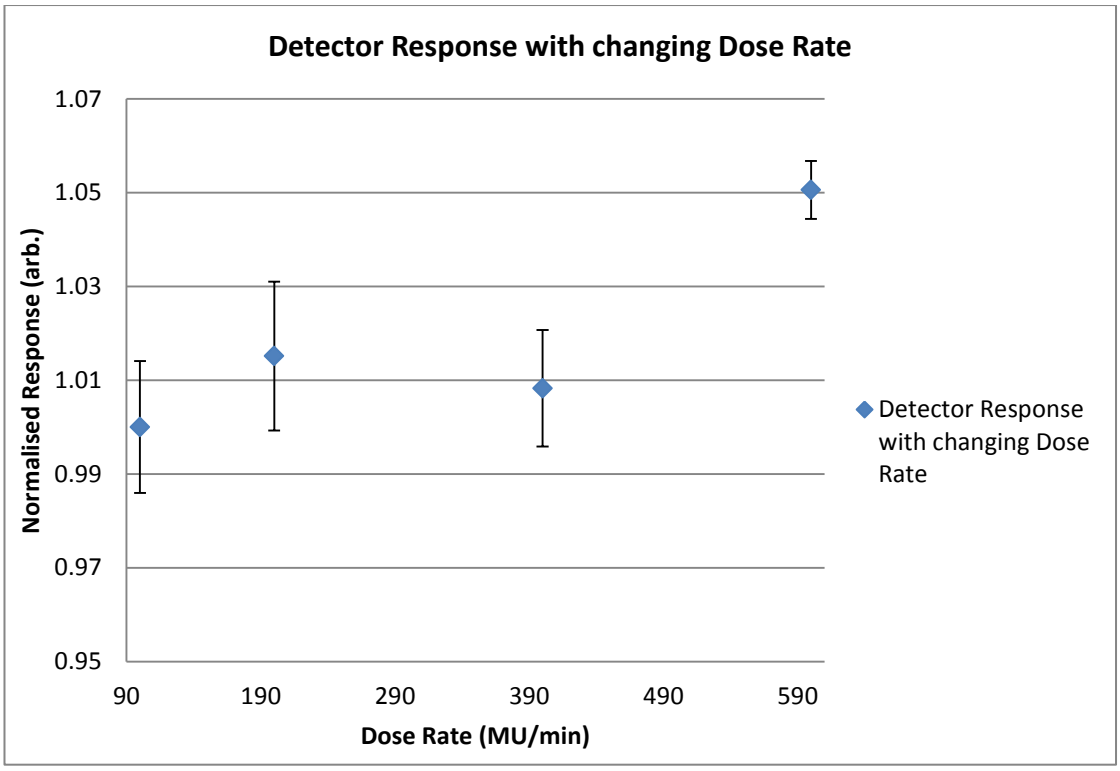

Figure 30: Dose rate dependence

Figure 30 shows the change in detector response with variation in dose rate, the signal has been normalised to 100MU/min and an increased response can be seen with increasing dose rate.

4.5.5 Discussion

The results of this experiment agree with those obtained by Viamonte, da Rosa, Buckley, Cherpak and Cygler [67] with almost identical results obtained within experimental error (95% confidence interval). This suggests that in the case of Al_2O_3:C NanoDot® OSLDS, a dose rate dependence can be observed and due to the statistical significance of this dependence, approximately 5%, the impact of dose rate will need to be considered to ensure accuracy and reliability in OSLD clinical use. The physical reason for this may be an increase in the rate of

electrons becoming trapped with a higher dose rate, this would give an increased signal at readout as a larger number of electrons would have become trapped.

4.6 Angular Dependence

4.6.1 Introduction

As discussed in 4.2.3, Al_2O_3:C OSLDs have been shown to vary in signal as much as 4% in a 6 MV clinical radiation beam. Given the primary application of these OSLDs will be for *in vivo* dosimetry and regions of interest on the patients' surface are rarely perpendicular to the beam, a thorough understanding of the angular dependence of OSLDs will be critical to their clinical use.

4.6.2 Aim

To examine the OSLDs at multiple angles to determine the magnitude of angular dependence.

4.6.3 Materials and Method

For this experiment a jig was fashioned out of solid water and Perspex to encase the OSLD and allow it to be positioned at a desired angle to the beam with a precision of 1^{o} (shown in Figure 32). The Perspex cylinder was machined to tightly fit an OSLD and fit inside the block of solid water, minimising air gaps. To ensure the cut-out within the cylinder was positioned directly below the centre of the solid water, (shown by the intersection of the black lines on the top of the block) a small steel ball used in clinical image registration was stuck in the cut-out and an image was obtained with the linacs' OBI and is shown in Figure 31 to be 0.03cm from precise centre.

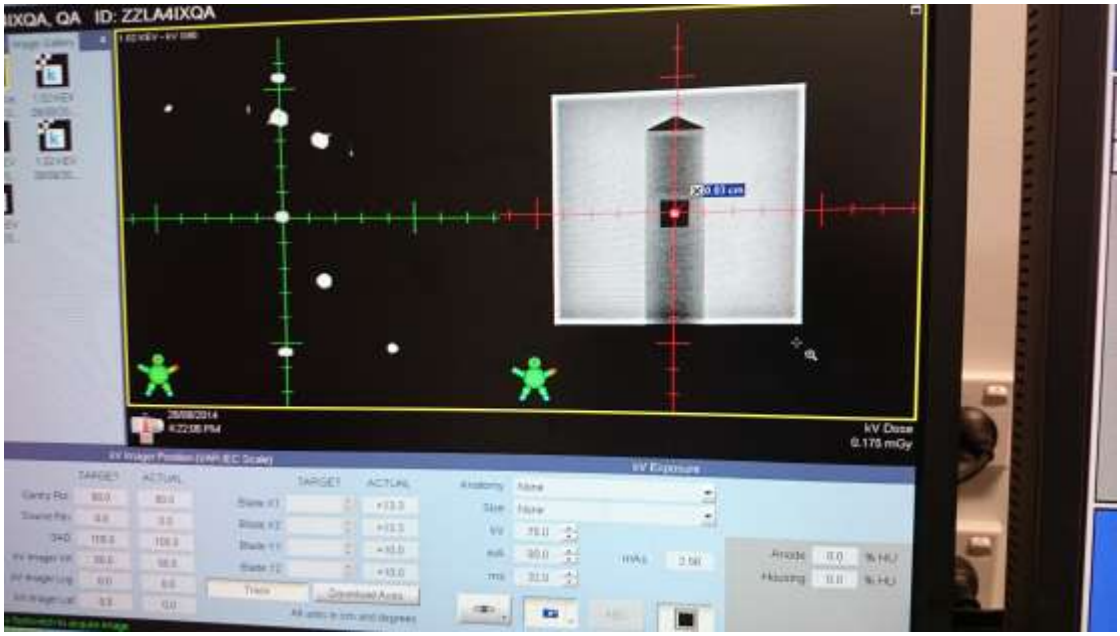

Figure 31: OBI image of steel fiducial in Perspex cylinder

Figure 32: Angular Dependence Jig (The University of Wollongong)

This jig was placed between two 10cm slabs of solid water in a 6cm x 6cm field at 6 MV and irradiated by 100MU as shown in Figure 33. A 6cm square field was chosen as the jig was 10cm x 10cm and due to setup geometry would have been outside the jig if a larger field was used.

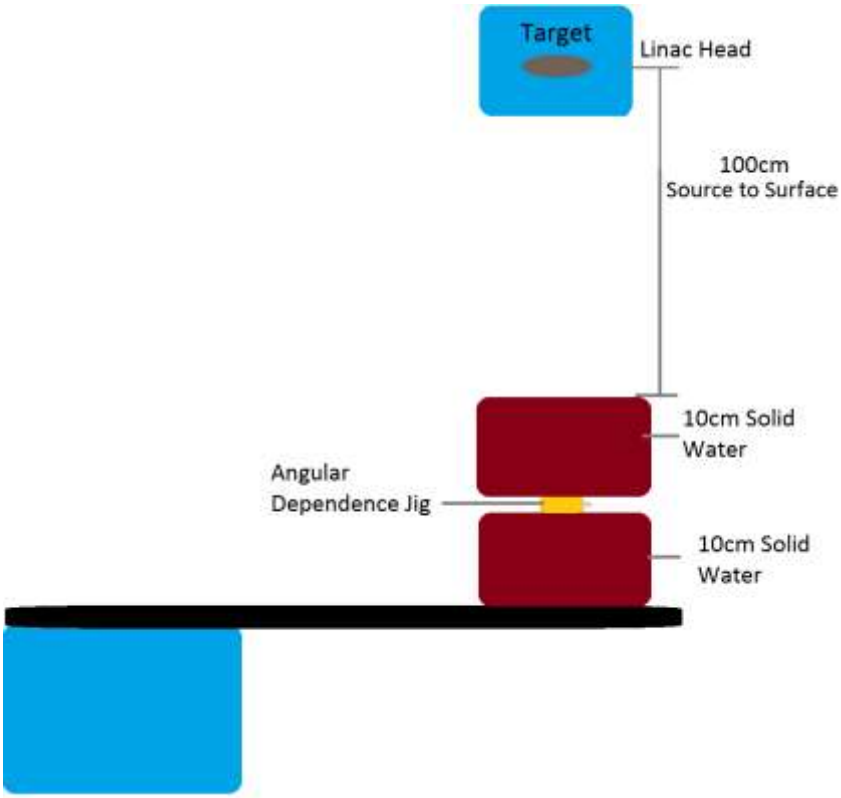

Figure 33: Angular Dependence Setup

Data points were obtained at 20 degree intervals around the entirety of the circle with three OSLDs used at each data point. As with previous measurements each OSLD was measured three times prior and post irradiation with the dose quoted the difference in the average of these readings. Due to the large number of readings and limited access time to the linac, the data was obtained in multiple sessions, as such each day a data point was obtained perpendicular to the machine for comparison.

4.6.4 Results

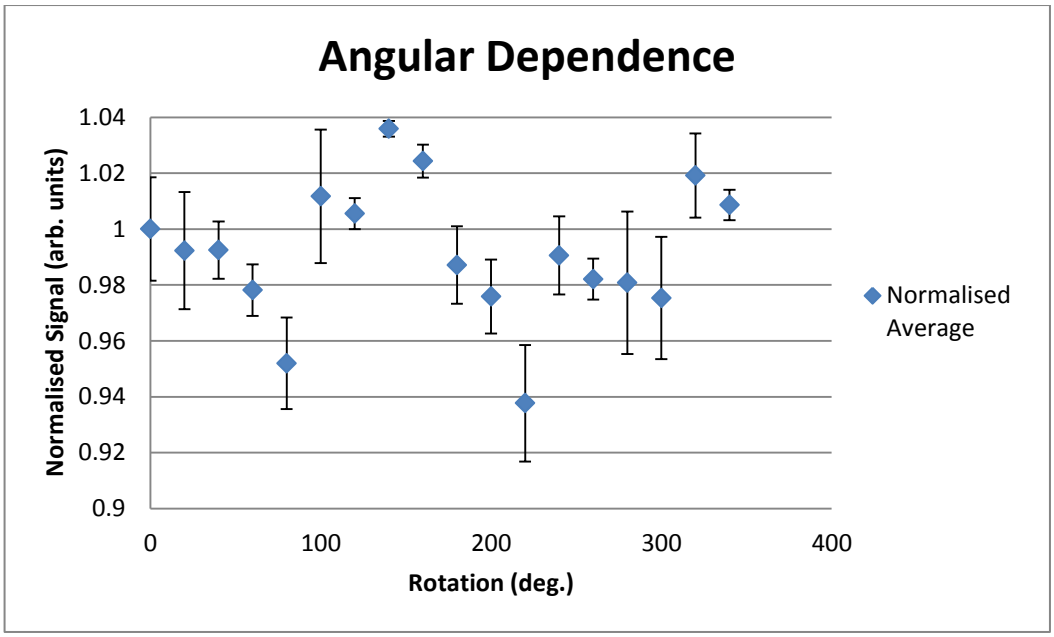

Figure 34: Angular Dependence of OSLDs

Figure 34 shows the variation of signal across 360° with error bars showing a 95% confidence interval. The variation of this data is 0.94-1.04 suggesting a ±4% range depending on the orientation of the dosimeter to the field.

4.6.5 Discussion

The result of this experiment (±4% angular dependence) agrees with those obtained by Kerns, Kry, Sahoo, Followill and Ibbott [58], Sharma and Jursinic [61] and Viamonte, da Rosa, Buckley, Cherpak and Cygler [67]. Jursinic [35] however, claims that OSLs have no angular dependence "within measurement uncertainty (0.9%)". The response in Figure 34 includes two regions of over response, between 100°-160° and between 320°-340°; this is either the result of low signal in the 0° reading to which subsequent reading are normalised to, or an unavoidable artefact of the chip construction which causes a different path length through plastic depending on the angle of the chip to the beam. Due to the symmetry of the OSLDs, the angular dependence around one axis can be used as the angular dependence in another.

4.7 Depth Dose Curve

4.6.6 Introduction

The use of OSLDs for *in vivo* measurements, particularly for those being used in clinical considerations, needs to be justified by their performance with little to no "build-up" material. The best way to examine this performance is through the creation of a depth dose curve and comparison with another *in vivo* dosimeter. By examining the build-up region of the depth dose curve the need for correction factors can be established or if required build-up caps can be fashioned to artificially improve a dosimeters' performance in the build-up region.

4.6.7 Aim

To examine the performance of OSLDs and EBT3 radiochromic film at a variety of depths.

4.6.8 Materials and Method

Figure 35 shows the experimental setup for the OSL investigation, the shaded solid water (maroon) was gradually increased in thickness with subsequent measurements while a 100cm SSD was maintained throughout the experiment. As the only previous method of reducing air gaps was a piece of SuperFlab© 1cm in thickness, a 1cm thick piece of solid water had a recess milled to precisely hold a single OSLD in the centre. This allowed pieces of solid water to be added in as little as 1mm increments from 2mm to 10cm with no significant air gaps.

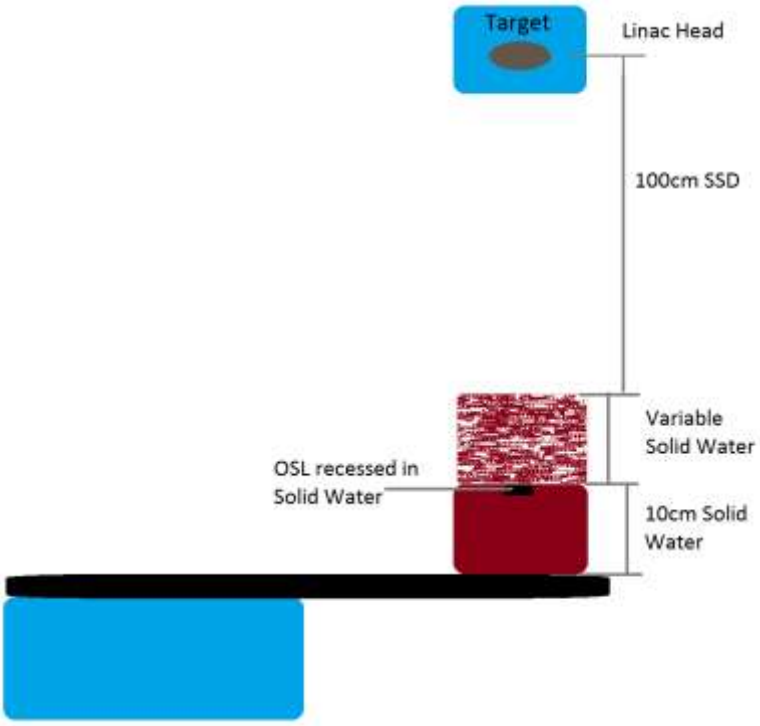

Figure 35: Depth Dose Setup

For comparison, EBT3 Gafchromic film was put through an identical experiment. Initially the film was prescanned 12 times and then cut into 3cm squares, 3 squares were used at each depth and the average dose was determined by post irradiation scanning and reading of the red channel counts. This number of counts in the red channel, was then converted to dose by comparison to a calibration curve obtained prior. This curve was obtained by using a known field setup giving a known dose and irradiating squares from the same piece of film at a range of known doses. Figure 36 shows an image of the sheet of EBT3 prior to prescanning with squares marked out showing 3cm squares.

For the Attix Ionisation Chamber measurements a 0.125cm^3 Gammex® Attix chamber was used, the experimental setup for this was identical to those using the Farmer chamber in previous experiments with a piece of recessed solid water removing air around the detector and an electrometer connected outside the room used to measure proportional charge.

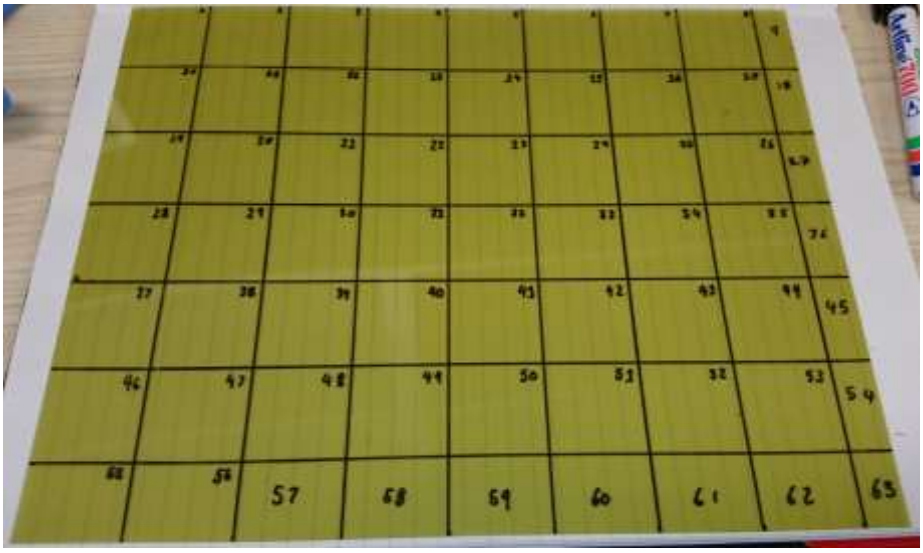

Figure 36: Sheet of EBT3 with 3cm grid marked out

4.6.9 Results

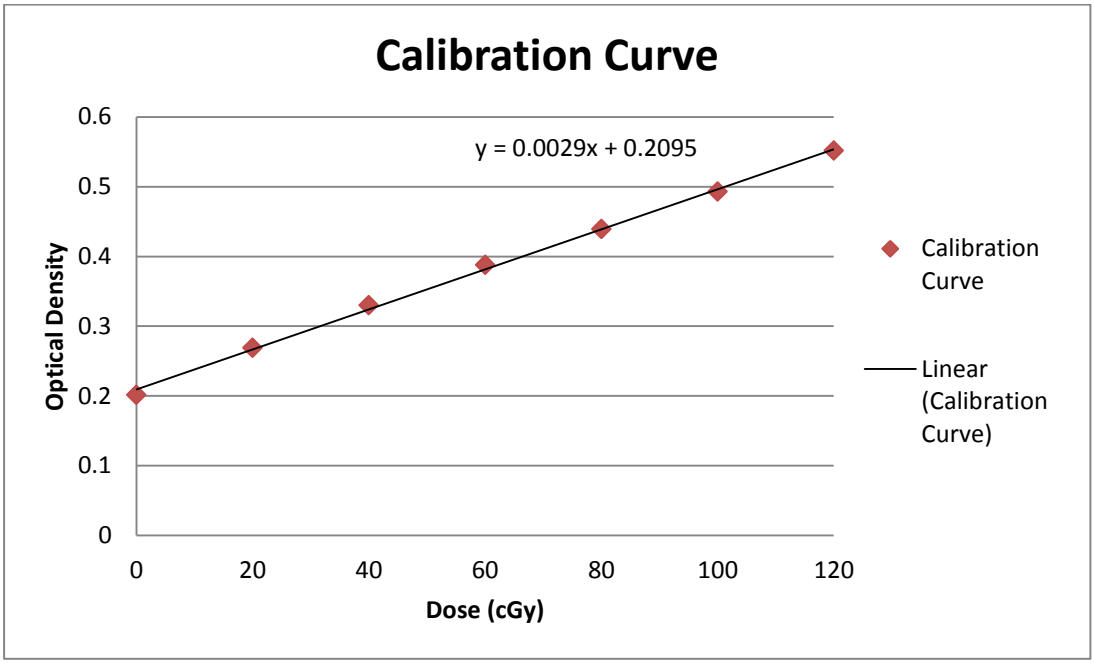

Figure 37: EBT3 Radiochromic film calibration curve (Maximum error 1%)

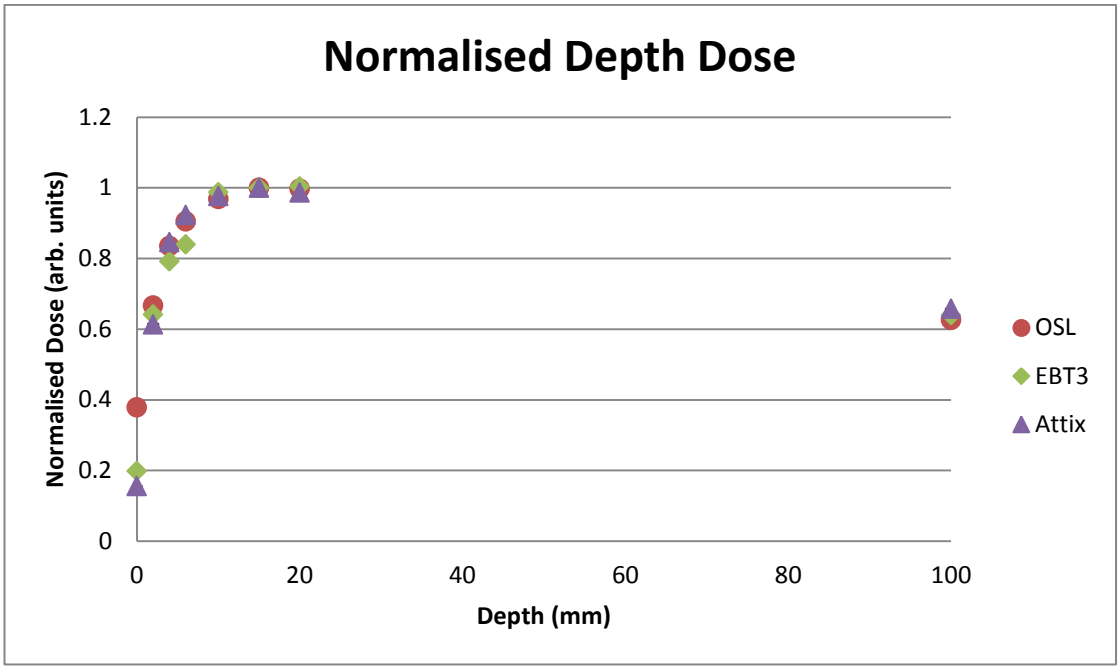

Figure 38: OSL, EBT3 and Attix Ion Chamber normalised depth dose at 6MV (95% conf. int. not visible)

4.6.10 Discussion

The calibration curve shown in Figure 37 was calculated using film squares cut from the same piece of film and irradiated at the same time as the film used to develop the depth dose curve. The setup in determining the calibration curve involved placing the film beneath 1.5cm of solid water and irradiating with known monitor units at 6MV. This arrangement was used as the linac being used was commissioned to deliver 1cGy/MU with this setup. The equation shown was then used to relate the optical density values in Figure 38 to dose as shown in Equation 29:

$$OD = (0.0029 * Dose) + 0.2095 \quad (29)$$

$$0.0029 * Dose = OD - 0.2095$$

Hence,

$$Dose = \frac{OD - 0.2095}{0.0029}$$

Equation 29: Relation between Optical Density (OD) and Dose for Calibration Curve

When presented as a normalised response on the same graph, as seen in Figure 38, the relative depth dose curve beyond 0mm is strikingly similar. Given the expected normalised response values based upon theory and other literature (see McCaw et al [73]), the agreement of these values provides reliability to the experimental procedure. The over response of the OSLDs at the surface is to be expected due to insufficient build up material being present.

For the Attix Chamber measurements, relative dose is the quoted value. This figure was determined by taking the average charge recorded at 10cm depth for a 10cm x 10cm field and dividing this value by 0.661, this value was determined at commissioning of the machine and corrects the 10cm deep value to d_{max}. Since the machine delivers 100cGy at d_{max} with a 10cm x 10 cm field, this charge value was then used as a known proportionality to convert the charge values measured to a relative dose in cGy. This was performed to provide an easier comparison with the OSL and EBT3 values. The results obtained by this method gave values accurate to other literature for depth dose curves with a d_{max} relative dose of 100.57cGy and a surface value of 15.49cGy [74].

5. MEPITEL® FILM

5.1 Effect of Mepitel® Film on surface dose

5.1.1 Introduction

Despite the massively positive effects of radiotherapy, a number of negative side effects can make treatment a difficult and trying process for patients who are already ill. Whilst treatments are designed to balance treatment effectiveness and a base level of patient comfort, improving patient comfort is always an excellent way of improving treatment.

Below are some common side effects of radiotherapy treatments, for each of these there is research into methods of reducing the both the severity and incidence rate. In addition to those listed, specific treatment sites each have their own complications and side effects [1, 75].

- Moist Desquamation: A painful condition caused as a result of severe damage to the basal cells of the skin. As a result of this damage the skin begins to ooze and can lead to infection at the affected area.
- Erythema: Reddening of the skin caused by radiation damage to the dermal or sub dermal layers of the skin.
- Change in hair colour or texture, including permanent hair loss
- Telangiectasia: Spider-web like marks on the skin from damage to superficial blood vessels.
- Lymphoedema: Blockage of the lymphatic system resulting in swelling of the extremities.
- Changes in fertility including permanent sterility

- Fibrosis (stiffening of tissue) causes a variety of complications depending on region affected including: regional swelling, shortness of breath, difficulty swallowing, incontinence and diarrhoea.
- Tiredness ranging in severity which often increases over treatment course

Skin cells are amongst the most sensitive to radiation and as a result, radiotherapy often causes complications with the patients' skin. One emerging technology for minimising the severity of radiotherapy induced skin conditions is Mepitel ® film. This film consists of a thin silicone film with an applied adhesive. The film protects the skin by maintaining a moist environment by allowing only excess moisture to evaporate without being non-permeable enough to protect from microbial contamination.

A recent phase iii trial by Herst, Bennett, Sutherland, Peszynski, Paterson and Jasperse [76] showed promising findings when using Mepitel® film compared to conventional topical treatments such as corticosteroids, hyaluronic acid and aloe vera. The patients who were treated with topical creams had radiation induced skin reactions that progressed to moist desquamation in 26% of patients. Only 44% of those patients who had the Mepitel® film applied during and post treatment developed any form of skin condition and none of these progressed to moist desquamation. However as shown in the previous chapter, in the first few millimetres of material there is significant build up in dose and although the film is extremely thin, the dose build-up of the material at least needs to be investigated. In addition to this the different mass energy absorption coefficient for the silicon of the film is different to the air and soft tissue on either side ($\frac{\mu_{en}}{\rho}$ for silicon is 0.01827cm^2g^{-1} compared to 0.01647 and 0.01786 cm^2g^{-1} for air and soft tissue respectively)[77]. Because of this, concern exists around the effect of using Mepitel® on the conformity of the dose and consequently the treatment effectiveness.

5.1.2 Aim

To determine if the application of Mepitel® Film on a patient, has significant effect on the surface dose to the area. Primarily through examination of the build-up effect of Mepitel® by using OSLDs.

5.1.3 Materials and Method

For this experiment, sequences of measurements were taken using both OSLDs and a Gammex® 0.125cc Attix Ionisation Chamber. 10cm of solid water was used as backscatter material and a 10cm x 10cm field at 100cm SSD was set up. 100MU were delivered with and without the presence of the film as well as a measurement at 10cm depth to provide a frame of reference. A 10cm x 10cm field at 100cm SSD was used as the linac had been calibrated to deliver 1cGy/MU with these settings. This process was then repeated at 10 MV to give a broader clinical relevance.

5.1.4 Results

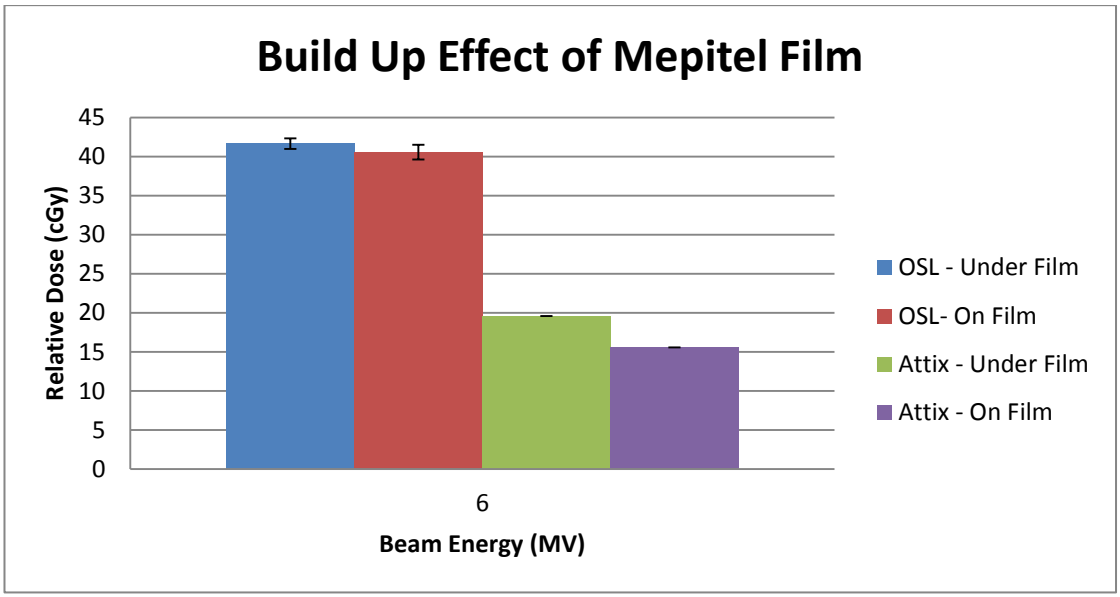

Figure 39: Build up effect of Mepitel® Film measured using OSL and Attix Ionisation Chamber (95% conf. int. shown)

5.1.5 Discussion

Figure 39 shows that Mepitel® has the effect of increasing surface dose to the patient, the degree to which this occurs however is not as clear. The OSLDs recorded an increase in dose from 40.555cGy to 41.646cGy for 6 MV. However, the Attix chamber recorded an increase of 15.584cGy to 19.587cGy for 6 MV. The Attix Chamber is commonly used for investigation in the build-up region and as such these values are likely more precise. The 25.68% increase measured by the Attix chamber is much closer than the OSLDs, to the 13% increase measured by Butson, Cheung, Yu and Metcalfe [78] for a 10cm x 10 cm field at 6 MV. Additionally Butson, et al. observed a decreased build up effect for the film with increasing field size and a decreased accuracy using TLDs compared to an Attix chamber. Another experiment conducted by Haas and Coletti [79] found an increase in skin bolus of 30-58% for a variety of dressings including Mepitel. Due to the nature of the publication however, no information could be obtained about equipment used or methodology.

6. CONCLUSION

The Landauer NanoDot® OSLD system has proven useful for radiotherapy treatment verification through several clinically desirable: The ease with which the system can become operational, the robustness of the OSLDs and the ease of readout are all beneficial properties of a clinical system.

Understanding the magnitude of factors affecting detector response is critical to accurate readings and consequently the value of OSLs to the treatment process as a whole. From investigation of the literature it was determined that short term fading, signal loss per readout, dose variation as well as linearity, dose rate, angular and depth dose dependence are all important quantities. In addition to this, operation of the Gammasonics® manual annealing lightbox and calculation of the relevant batch sensitivity values were investigated to ensure completeness of this study.

The values of the quantities mentioned fell within acceptable limits when compared with other dosimeters and previous NanoDot® investigations. This suggests that in terms of dose accuracy, OSLDs are at worst comparable with currently used technology. The 164% over response in the first 2mm and the ±4% angular dependence are both of particular relevance when NanoDots® are used for *in vivo* measurements. The signal measured shows excellent stability after a 20% decrease over the first 30 minutes and can be read multiple times with only a 0.05% decrease in signal per readout. The 5% dose rate dependence and variation over multiple readouts are both useful quantities to know.

When applied to a clinical investigation, it was found that Mepital® film caused an increase in build-up of surface dose. Although the magnitude determined of this increase by OSL investigation disagreed with previous studies, this may be attributed to the effects of the construction.

With careful setup, including the determination of an appropriate calibration factor, as well as occasional QA checks, using the calibrated NanoDots® to provide adequate dose accuracy is possible. With dose values theoretically as accurate as a ten thousandth of a Gray possible and a readout procedure of only a few seconds, the NanoDot® system allows the end user to determine the accuracy of their system based on needs.

For day to day use of NanoDots® with minimal time investment into set up and calibration, whilst still accounting for the wide number of factors affecting dose accuracy, a dose accuracy of 5% should be expected. This is based on a 36hr anneal to ensure a initial dose of no more than 0.1cGy and a readout procedure involving the averaging of 3 readouts following a 30 minute waiting period. For simple clinical investigation this is anticipated to be sufficient with more accurate readings shown to be possible with a greater time investment.

7. REFERENCES

[1] Cancer Council Australia, Facts and Figures, in, 2014.
[2] N.o.N.M. AB, Wilhelm Conrad Rontgen - Biographical, in, 2014.
[3] I.C.o.R. Protection, The 2007 Recommendations of the International Commission on Radiological Protection - ICRP Publication 103, in: J. Valentin (Ed.) Annals of the ICRP, 2007.
[4] N.C. Institute, Radiation Therapy for Cancer, in, 2010.
[5] E. Podgorsak, Radiation oncology physics: A handbook for teachers and students, International Atomic Energy Agency, Vienna, 2005.
[6] Elsevier, Dorland's Medical Dictionary for Health Consumers, in, 2007.
[7] P. Metcalfe, T. Kron, P. Hoban, The physics of radiation therapy: X-rays and electrons, Medical Physics Publishing, Madison, 2007.
[8] G. Knoll, Radiation detection and measurement, John Wiley & Sons, Inc, New York, 2000.
[9] J. Izewska, G. Rajan, Radiation Dosimeters, in: Radiation Oncology Physics: A handbook for teachers and students, International Atomic Energy Agency, Heidelberg, 2007.
[10] P. Mayles, A. Nahum, J.C. Rosenwald, Handbook of Radiotherapy Physics: Theory and Practice, Taylor & Francis, Boca Raton, 2007.
[11] C. Kalnins, H. Ebendorff-Heidepriem, N. Spooner, T. Monro, Optically Stimulated Luminescence in Fluoride-Phosphate Glass for Radiation Dosimetry, Journal of American Ceramic Society, 94 (2010) 474-474.
[12] S. Miller, High dose dosimetry using optically stimulated luminescence, Radiation Protection Dosimtery, 66 (1996) 201-204.
[13] E. Yukihara, Luminescence properties of BeO Optically Stimulated Luminescence (OSL) detectors, Radiation Measurement, 46 (2011) 580-587.
[14] R. Evans, The Atomic Nucleus, McGraw-Hill, New York, 1955.
[15] F. Attix, Introduction to Radiological Physics and Radiation Dosimetry, John Wiley & Sons, Inc., Weinheim, 1986.
[16] NIST, Tables of X-Ray Mass Attenuation Coefficients and Mass Energy-Absorption Coefficients from 1 keV to 20 MeV for Elements Z = 1 to 92 and 48 Additional Substances of Dosimetric Interest*, in, 2009.
[17] W. Mayneord, The significance of the rontgen, Acta Int Union Against Cancer, 2 (1937) 271.
[18] M. Taylor, Effective Atomic numbers of cancerous tissues, Journal of Medical Physics, 39 (2012a) 5436-5445.
[19] M. Taylor, R. Smith, F. Dossing, R. Franich, Robust calculation of effective atomic numbers: The Auto-Zeff software, American Association of Physicists in Medicince, 39 (2012b) 1769-1779.
[20] H. Manjunatha, B. Rudraswamy, Study of effective atomic number and electron density for tissues from human organs in the energy range of 1keV-100Gev, Health Physics Society, 104 (2013) 158-162.
[21] S. Manohara, S. Hanagodimath, K. Thind, L. Gerward, The effective atomic number revisited in the light of modern photon-interaction cross-section databases, Applied Radiation and Isotopes, 68 (2010) 784-787.
[22] F. Kahn, The Physics of Radiation Therapy, Maple Press, Philadelphia, 2003.
[23] J. Bushberg, J. Seibert, E. Leidholdt, J. Boone, The Essential Physics of Medical Imaging, Lippincott Williams & Wilkins, Philadelphia, 2012.
[24] J. HE, C. JR, The Physics of Radiology, Fourth ed., Charles C Thomas, Springfield, Illinois, 1983.
[25] R. Mohan, C. Chui, Energy and angular distributions of photons from medical linear accelerators, Medical Physics, 12 (1985) 592-597.

[26] L.B. Levy, R.G. Waggener, A.E. Wright, Measurement of primary bremsstrahlung spectrum from an 8MeV linear accelerator, Medical Physics, 3 (1976) 173-175.
[27] M. Sommer, J. Henniger, Investigation of a BeO-Based optically stimulated luminescent dosemeter, Radiation Protection Dosimetry, 119 (2006) 394-397.
[28] C. Salle, P. Grosseau, B. Guilhot, P. Iacconi, M. Benabdesselam, G. Fantozzi, Detection of tetragonal zirconia in alumina-zirconia powder by thermoluminescence, Journal of the European Ceramic Society, 23 (2002) 667-673.
[29] W. Pingqiang, C. Zhaoyang, F. Yanwei, S. Turun, Z. Yun, Dose rate dependence of optically stimulated luminescence, Journal of Semiconductors, 31 (2010) 102001-102001-102004.
[30] E. Yukihara, P. Gasparian, Sawakuchi, GO, C. Ruan, S. Ahmad, C. Kalvagunta, W. Clouse, N. SAhoo, U. Titt, Medical applications of optically stimulated luminescence detectors (OSLDs), Radiation Measurements, 45 (2010) 658-682.
[31] E. Yukihara, G. Mardirossian, M. Mirzasadeghi, S. Guduru, S. Ahmad, Evaluation of Al_2O_3:C optically stimulated luminescence (OSL) dosimeters for passive dosimetry of high energy photon and electron beams in radiotherapy, Medical Physics, 35 (2008) 260-269.
[32] Dictionary.com, in vivo, in, 2009.
[33] ICRU, Determination of absorbed dose in a patient irradiated by beams of X or gamma rays in radiotherapy procedures, in: ICRU, International Comission on Radiological Protection, Bethesda, Maryland, 1976.
[34] T. Kron, Thermoluminescence dosimetry and its applications in medicine - Part 2: History and applications, Australa Phys Eng Sci Med, 18 (1995) 1-25.
[35] P. Jursinic, Characterization of optically stimulated luminescent dosimeters, OSLDs, for clinical dosimetric measurements, Journal of Medical Physics, 34 (2007) 4594-4604.
[36] J.T.W. Randall, M. H. F, Phosphorescence and electron traps II. The interpretation of long-period phosphorescence, Proceedings of the Royal Society London, Series A: Mathematical and Physical Sciences, 184 (1945) 390-407.
[37] J.A. Harvey, N.P. Haverland, K.J. Kearfott, Characterization of the glow-peak fading properties of six common thermoluminescent materials, Applied Radiation and Isotopes, 68 (2010) 1988-2000.
[38] M. Moscovitch, Y.S. Horowitz, Thermoluminescent materials for medical applications: LiF:Mg,Ti and LiF:Mg,Cu,P, Radiation Measurement, 41 (2007) S71-S77.
[39] A. McKinlay, Thermoluminescence Dosimetry, Adam Hilger, Bristol, UK, 1981.
[40] R. Chen, Kinetics of thermoluminescence glow peaks, in: Y.S. Horowitz (Ed.) Thermoluminescence and Thermoluminescent Dosimetry, CRC Press, Boca Raton, Florida, 1984.
[41] L.Z. Luo, Long term study of Harshaw TLD LiF– LLD and uncertainty, Radiation Measurements, 45 (2010) 569-572.
[42] K. Nakagawa, H. Koyanagi, T. Shiraki, S. Saegusa, K. Sasaki, T. Oritate, K. Mima, M. Miyazawa, T. Ishidoya, K. Ohtomo, K. Yoda, A radiophotoluminescent glass plate system for medium-sized field dosimetry, Review of Scientific Instruments, 76 (2005) 106104(106101)-106104(106104).
[43] S.-M. Hsu, H.-W. Yang, T.-C. Yeh, W.-L. Hsu, C.-H. Wu, C.-C. Lu, W.-L. Chen, D.Y.C. Huang, Synthesis and physical characteristics of radiophotoluminescent glass dosimeters, Radiation Measurements, 42 (2007) 621-624.
[44] J. Van Dyk, Modern Technology of Radiation Oncology: A Compendium for Medical Physicists and Radiation Oncologists, Medical Physics Publishing, Madison, Wisconsin, 1999.
[45] M. Butson, T. Cheung, P.K.N. Yu, Weak energy dependence of EBT gafchromic film dose response in the 50kVp-10MVp X-ray range, Applied Radiation and Isotopes, 64 (2006) 60-62.

[46] C. Soares, Radiochromic Film, in, National Institute of Standards and Technology, Gaithersburg, MD, 2009.
[47] C. Baldock, Y. De Deene, S. Doran, G. Ibbott, A. Jirasek, M. Lepage, K. McAuley, M. Oldham, L. Schreiner, Polymer Gel Dosimetry, Physics Medicine Biology, 55 (2010) R1-R63.
[48] IAEA, TRS-398, in, International Atomic Energy Agency, Vienna, 2006.
[49] G.T. Betzel, S.P. Lansley, F. Baluti, L. Reinisch, J. Meyer, Clinical investigations of a CVD diamond detector for radiotherapy dosimetry, European Journal of Medical Physics, 28 (2011) 144-152.
[50] R. Ramani, S. Russell, P. O'brien, Clinical Dosimetry using MOSFETs, International Journal of Radiation Oncology Biology Physics, 37 (1997) 959-964.
[51] M. Butson, A. Rozenfeld, J. Mathur, M. Carolan, T. Wong, P. Metcalfe, A new radiotherapy surface dose detector: The MOSFET, Medical Physics, 23 (1996) 655-658.
[52] A.R. Barron, Chemistry of the Main Group Elements, in: Applications for Silica Thin Films, Openstax CNX, 2010.
[53] R. Boellaard, M. Essers, M. Van Herk, B.J. Mijnheer, New method to obtain the midplane dose using portal in vivo dosimetry, international Journal of Radiation Oncology Biology Physics, 41 (1998) 465-474.
[54] M. Wendling, R.J.W. Louwe, L.N. McDermott, J.-J. Sonke, M. van Herk, B.J. Mijnheer, Accurate two-dimensional IMRT verification using a back-projection EPID dosimetry method, International Journal of Medical Physics, 33 (2006) 259-273.
[55] E. Yukihara, S. McKeever, Optically stimulated luminescence (OSLD) dosimetry in medicine, Physics in Medicine and Biology, 53 (2008) 351-379.
[56] I. Mrcela, T. Bokulic, J. Izewska, M. Budanec, A. Frobe, Z. Kusic, Optically stimulated luminescence in vivo dosimetry for radiotherapy; physical characterization and clinical measurement in Co-60 beams, Journal of Physics Medicine Biology, 56 (2011) 6065-6082.
[57] R. Al-Senan, M. Hatab, Characteristics of an OSLD in the diagnostic energy range, Journal of Medical Physics, 38 (2011) 4396-4406.
[58] J. Kerns, S. Kry, N. Sahoo, D. Followill, G. Ibbott, Angular Dependence of the nanoDot OSL dosimeter, Journal of Medical Physics, 38 (2011) 3955-3963.
[59] L.C. Baird, D.R. White, A survey of tissue substitutes and phantoms in 98 US centers, Medical Physics, 9 (1982) 434-435.
[60] T. Kron, P. Metcalfe, J.M. Pope, Investigation of the tissue equivalence of gels used for NMR dosimetry, Phys. Med. Biol., 38 (1993) 139-150.
[61] R. Sharma, P.A. Jursinic, In vivo measurements for high dose rate brachytherapy with optically stimulated luminescent dosimeters, American Association of Physicists in Medicine, 40 (2013) 071730-071731 - 071730-071712.
[62] L. Dunn, J. Lye, J. Kenny, J. Lehmann, I. Williams, T. Kron, Commissioning of optically stimulated luminescence dosimeters for use in radiotherapy, Radiation Measurements, 51 (2013) 31-39.
[63] G. Australia, OSL Annealing Lightbox User Manual, in, Gammasonics, 2011, pp. 6.
[64] M. Phipps, M.P. Quine, Primer of Statistics, 4th ed., Prentice-Hall, 2001.
[65] E. Yukihara, S. McKeever, Optically Stimulated Luminescence: Fundamentals & Applications, John Wiley & Sons Ltd, Chichester, 2011.
[66] M.S.B.-J. Akselrod, L; McKeever, S.W.S., Optically stimulated luminescence and it's use in medical dosimetry, Radiation Measurement, 41 (2007) S78-S99.
[67] A. Viamonte, L.A.R. da Rosa, L.A. Buckley, A. Cherpak, J.E. Cygler, Radiotherapy dosimetry using a commercial OSL system, American Association of Physicists in Medicine, 35 (2008) 1261-1266.
[68] L. Botter-Jensen, S.W.S. McKeever, A.G. Wintle, Optically Stimulated Luminescence Dosimetry, Elsevier Science, Amsterdam, 2003.

[69] Workcover NSW, Guidlines on working in cold conditions, in, NSW Nurse and Midwives association, Sydney, 2009.
[70] P.V. Muriel, Hypofractioniation in radiotherapy, Clin Transl Oncol, 9 (2007) 21-27.
[71] B. Hu, Y. Wang, W. Zealey, Performance of Al2O3:C optically stimulated luminescence dosimeters for clinical radiation therapy applications, Australasian Physical & Engineering Sciences in Medicine, 32 (2009) 226-232.
[72] R. Chen, P.L. Leung, Nonlinear dose dependence and dose-rate dependence of optically stimulated luminescence and thermoluminescence, Radiation Measurements, 33 (2001) 475-481.
[73] T.J.M. McCaw, J.A; DeWerd, L.A, Development and Characterization of a three dimensional radiochromic film stack dosimeter for megavoltage photon beam dosimetry, Medical Physics, 41 (2014) 052104-052101 - 052104-052114.
[74] AAPM, AAPM's TG-51 Protocol for clinical reference dosimetry of high-energy photon and electron beams, Medical Physics, 30 (1999) 722-723.
[75] Cancer Research UK, Long Term Side Effects of Radiotherapy, in, 2014.
[76] P. Herst, N. Bennett, A. Sutherland, R. Peszynski, D. Paterson, M. Jasperse, Prophylactic use of Mepitel Filkm prevents radiation-induced moist desquamation in an intra-patient randomised controlled clinical trial of 78 breast cancer patients, Radiotherapy and Oncology, 110 (2014) 137-143.
[77] J. Hubbell, S. Seltzer, Tables of X-Ray Mass Attenuation Coefficients and Mass Energy-Absorption Coefficients from 1keV to 20MeV for Elements Z=1 to 92 and 48 Additional Substances of Dosimetric Interest, in, National Institute of Standards and Technology - Physical Measurement Laboratory, Gaithersburg, 2004.
[78] M. Butson, T. Cheung, P. Yu, P. Metcalfe, Measurement of skin dose variations produced by a slicon-based protective dressing in radiotherapy, Phys. Med. Biol., 47 (2002) N145-N151.
[79] M. Haas, J. Coletti, Managing Skin Reaction From Radiation or Combined Chemoradiation Therapy, International Journal of Radiation Oncology, 69 (2007) S560-S560.